**PhD Dissertation**

**博士学位論文**

---

# Single cell transcriptomics reveals a fate transitioning factor of cardiomyocytes in mitochondrial cardiomyopathy

## 1 細胞発現解析により見出したミトコンドリア心筋症の病態進行因子の同定

---


Osaka University – Department of Frontier Biosciences

大阪大学　生命機能研究科

Tasneem　Qaqorh


（令和 5 年　3 月 22 日　修了見込）


Professor Takashima Seiji

高島成二　教授

# Abstract

Mitochondrial diseases (MDs) are complicated disorders caused by mutations in genes essential for mitochondrial function and have a high prevalence, the most prevalent of which are mutations in complex I of the electron transport chain. OXPHOS dysfunction is a tightly regulated process that activates cascades of cellular regulatory mechanisms that often cannot be sustained due to constant metabolic perturbation. Previous research on MD has focused on late stages or phenotypes with more severe tissue dysfunction, making it difficult to identify factors that shut down endogenous maintenance pathways and direct cells to malfunction. Furthermore, CI dysfunction has not been studied and the underlying mechanisms involved in pathogenesis are not well understood, particularly in the context of cardiomyopathy. The aim of this study was to identify such factors and how they contribute to cellular-specific switching to maladaptive state. Therefore, I utilized single cell transcriptomics on hearts of CI *Ndufs6*-deficient (FS6KD) female mice, showing cardiac specific phenotype worsening with age, then analyzed using ScanPY analytical platform to perform integration, clustering, differential gene expression analysis, gene ontology, and finally PAGA pseudotime trajectory. The results showed CI-dysfunction in the heart promotes *Pgc1a* upregulation to act as the initial endogenous adaptation response, regulating mitochondrial biogenesis and glucose metabolism. Suppression of Pgc1a expression was found to be a crucial point for tissue transitioning to malfunction. In cardiomyocytes, I was able to capture the dynamic transcriptional reprogramming underlying this transitioning within subclusters of young FS6KD, modulated by transient expression of a key transcription factor acting as a repressor. Adaptive mechanisms were found to be activated following shutdown of this early response, suggesting the role of the repressor as a fate determining factor. Early endogenous Pgc1a upregulation followed by shutdown was shared among cardiac cellular populations but was not modulated by the same factors identified in cardiomyocytes. In conclusion, these findings support the importance of cellular resolutions in understanding heterogeneous disorders such as MDs, and in identifying targets for therapy.

# Table of contents

# List of figures

# List of Tables

# Abbreviation glossary

| | |
|---|---|
| Ankrd1 | Ankyrin repeat domain-containing protein 1 |
| Atf3 | Activating transcription factor 3 |
| Atf4 | Activating transcription factor 4 |
| Atf5 | Activating transcription factor 5 |
| Atf6 | Activating transcription factor 6 |
| Cdh4 | Cadherin 4 |
| ddPCR | Droplet digital PCR |
| DEG | Differentially expressed genes |
| EF | Ejection fraction |
| FS6KD | Ndufs6 knockdown |
| GO | Gene ontology |
| Il6 | Interleukin 6 |
| $ISR^{mt}$ | Mitochondrial integrated stress response |
| $Log_2FC$ | log2-foldchange |
| LVID;d | Left ventricular internal diameter end diastole |
| MD | Mitochondrial disease |
| mtDNA | Mitochondrial DNA |
| nDNA | Nuclear DNA |
| Ndufs6 | NADH:Ubiquinone oxidoreductase subunit S6 |
| Nppa | Natriuretic peptide A |
| Nppb | Natriuretic peptide B |
| OXPHOS | Oxidative phosphorylation |
| Pgc1a | Peroxisome proliferator-activated receptor gamma coactivator 1-alpha |
| Serpine1 | Serpin family E member 1 |
| SMC | Smooth muscle cells |
| snRNA-seq | single nucleus RNA sequencing |
| TF | Transcription factor |
| TnnI3 | Troponin I3, cardiac type |
| UMAP | Uniform manifold approximation and projection |
| $UPR^{mt}$ | Mitochondrial unfolded protein response |
| WT | Wild type |
| Xirp2 | Xin actin binding repeat containing 2 |

# Introduction and literature

Mitochondria have been "under the microscope" in the past few decades where they have been extensively studied for their complexity and importance. Although always referred to as the powerhouse of the cell, they are multi-functional organelles playing roles exceeding the frontier of energetics, such as apoptosis and cell signalling, to name a few. Mitochondria are double membranous organelles which contain their own circular, double-stranded genome, called mitochondrial DNA (mtDNA)[1,2]. It is approximately 16.6 kilobase pair long and contains 37 genes, only 13 of which encode proteins, while the rest of the 1500 mitochondrial proteins are encoded by nuclear DNA (nDNA)[3–5]. These proteins are imported into the mitochondria and are assembled into different compartments and into different protein complexes[6]. Other genes encode for transfer RNAs (tRNAs) and ribosomal RNAs (rRNAs)[7].

## Role of mitochondria in energy production

The most prominent role of mitochondria is undeniably aerobic respiration and energy production (Fig.1). This process takes place in several cell compartments and is fuelled by the oxidation of different macromolecule precursors such as carbohydrates and lipids. In the cytosol, sugars are transformed into pyruvate by a multi-step process known as glycolysis. Pyruvate is then transported to the mitochondrial matrix, where the Krebs cycle, also known as the tricarboxylic acid cycle (TCA), is in operation. Pyruvate is transformed into acetyl-coA, which enters the cycle and results in the release of free energy in the form of electrons, which is captured by electron carriers such as NADH and FADH2. Fatty acids, a more efficient energy source, are converted to acetyl-coA by beta-oxidation process in the mitochondria. The final and possibly most crucial phase is oxidative phosphorylation (OXPHOS). Electron carriers deliver these electrons to the electron transport chain (ETC) or respiratory chain (RC), which facilitates the formation of a proton gradient across the inner mitochondrial membrane (IMM). The ETC is made up of five complexes that contain roughly 90 proteins required for proper function and assembly. These proteins are encoded by genes on both mtDNA and nDNA, with the exception of complex II, which is exclusively composed of nDNA-encoded proteins, emphasizing the complexity of OXPHOS. Electrons are transferred to complex 1, or NADH dehydrogenase, the largest and main electron entry point into the chain, which then transfers them to coenzyme Q. Complex II, succinate dehydrogenase, can also receive FADH2 electrons and reduce coenzyme Q. Electrons are next carried to cytochrome c reductase (complex III), then to cytochrome *c*, and lastly to cytochrome *c* oxidase (complex IV). At complex IV, electrons are used to reduce oxygen to water. The passage of electrons through the ETC releases energy, which is coupled to protons pumping into the intermembrane space by complexes I, III, and IV, resulting in a chemical gradient. Protons flow down the gradient through complex V, ATP synthase, or F0F1 ATPase, back to the matrix, generating rotational movement and conformational change, which leads to the conversion of ADP to ATP in the last step of OXPHOS[8,9].

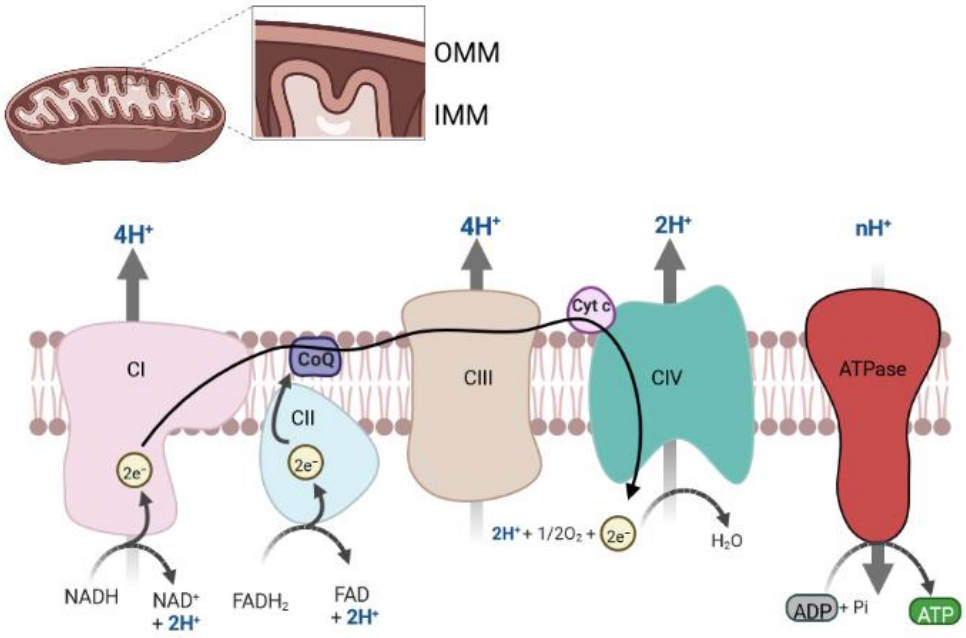


**Fig 1 Mitochondrial ETC**.

Transfer of electrons from electron carriers to complexes I-IV for the reduction of molecular oxygen to water. Pumping protons by complexes I, III, and IV create a proton gradient used to create ATP by ATP synthase. Created with BioRender.com

## Regulation of OXPHOS and mitochondrial diseases

The production of energy by OXPHOS is a tightly regulated process and all protein complexes need to be correctly assembled and embedded in the IMM. Expression of OXPHOS proteins encoded by the mitochondrial genome occurs inside the mitochondria[10] and are translated by mitochondrial ribosomes (mitoribosomes)[11,12], but the other nuclear-encoded proteins are transcribed and translated in the cytosol and then transported into the mitochondria for assembly with mitochondrial proteins. This requires a high level of regulation to ensure that nuclear-transcribed mRNAs are exported to the cytosol, translated, and then imported into the mitochondria[12]. Communication between nucleus and mitochondria is thus necessary, achieving balance between energetic demands of the cell and the energetic resources present at any given time[13]. Defects in OXPHOS arising from mutations in genes encoded by mtDNA or nDNA, result in metabolic deficiency leading to mitochondrial disorders (MDs). Genes involved in OXPHOS are genes encoding ETC complexes enzymes, their assembly factors, proteins important in mitochondrial or nuclear translational machineries, transcription machineries, proteins involved in early steps of respiration, cofactors of OXPHOS, import and export, or mitochondrial quality control and homeostasis[14]. MDs are a heterogeneous group of genetic diseases with several modes of inheritance, and broad pleiotropic or isolated clinical phenotypes that can manifest in early

childhood or adulthood[15,16]. Although a MD caused by nDNA mutations follows Mendelian inheritance, mtDNA mutations are strictly maternally inherited; since paternal mitochondria do not enter the oocyte or are destroyed after fertilization[17]. Higher degree of complexity is also introduced due to heteroplasmic nature of mitochondrial genomes. Mutated mitochondria more commonly exist in a mixture with wildtype mitochondria, and this mixture differs in different cells, tissues and even at different times in a patient's life[16]. Phenotype and disease intensity are dependent on the level of heteroplasmy, where there should be enough percentage of mutated mtDNA to induce development of clinical features. This is known as the threshold effect[18], and while it varies among tissues, a load of more than 60% is usually required[19] for disease manifestation.

## Clinical manifestations

Clinical outcomes of mitochondrial defects are observed in all tissues, particularly in high energy-demanding systems such as the central nervous system, cardiovascular, muscular, and gastrointestinal. MDs are heterogeneous genotypically and phenotypically with wide range of symptoms, such as weakness, seizures, myopathies, muscle weakness, hearing loss, vision loss, and failure in tissues affected. Most common paediatric or early-onset MDs are Leigh syndrome and mitochondrial encephalomyopathy, lactic acidosis, and stroke like episodes (MELAS). Other early-onset syndromes include Leber's hereditary optic neuropathy (LHON), myoclonic epilepsy with ragged red fibres (MERRF), Kearns-Sayre syndrome (KSS), mitochondrial DNA depletion syndrome (MDS), Neuropathy, ataxia, and retinitis pigmentosa (NARP), and Pearson syndrome[20–26]. MDs developed in adults or showing a later onset often show much broader, progressive, and multi-systemic phenotype[27]. Notably, these manifestations are not caused by a single gene. The most common pathogenic mutation, m.3243A>G in the tRNA MT-TL1 gene, causes pleiotropic phenotypes and has been linked to a wide range of disorders[28,29]., while Leigh syndrome is caused by at least 89 genes involved in mitochondrial function[30].

## Prevalence of mitochondrial diseases

Earlier studies on epidemiology in general populations claimed a frequency of roughly 1 in 5000 people or less[31,32]. However, various restrictions exist when determining whether individuals have a MD, ultimately reflecting incorrectly the true prevalence in any group. Previous estimates focused solely on frequent pathogenic mutations, mostly arising from mutations in mitochondrial genome, therefore they did not provide a population-wide perspective. Additionally, the heterogeneity of genotypes and clinical phenotypes of these disorders might have rendered many symptoms as non-specific, or attributed to other clinical diagnoses and overlooked, further underestimating the true frequency of such diseases. Diagnostic approaches offered additional limitation in appropriately detecting complex nDNA mutations, especially since Next Generation Sequencing (NGS) tools were not available at the time[33]. Early numbers also reflected patients who were referred to further diagnoses based on severe clinical symptoms, not taking in consideration individuals who

are heteroplasmic for pathogenic mutations, also called carriers or "at-risk", that can develop late onset of the disease. Several cohort studies over the past two decades aimed to determine a more comprehensive prevalence of MDs in different populations. Over a period of 8 years in British Columbia[34], a study including at least 400,000 children estimated respiratory chain (RC) disorders to be about 3 in 100,000. This estimate was about three times higher in the same demographic in a study done in Western Sweden[35]. Period prevalence of mitochondrial encephalomyopathies in children under 6 years was estimated 8.9 in 100,000, while a point prevalence of children under 16 years was 4.8 in 100,000. Similar frequency of 5 in 100,000 births was reported in South-eastern Australia[36] for the same period. Incident rate significantly increased for about 21% of the studied population that were of Lebanese origin, estimated with 58.6 in 100,000 minimum births. Although they included dual genome mitochondrial disorders, these studies were done on patients younger than 16 years with definite diagnosis and showing evident clinical phenotypes. A cohort studies on adults with MDs were based in Northeast of England[37] reported a minimum 15-year period prevalence of 9.18 in 100,000 patients with MDs of single mtDNA mutation. They also reported a higher minimum prevalence of 16.5 in 100,000 for clinically unaffected but at-risk individuals. Although Incident of healthy carrier individuals of mtDNA mutations was reported about 1 in 200 in another UK study the same year[38]. The most comprehensive report on epidemiology in adult population of Northeast England estimated the total prevalence to be 23 in 100,000, or equal to 1 in 4300, clinically affected by either mtDNA or nDNA mutations[39]. Patients affected with mtDNA mutations showed 9.6 in 100,000-point prevalence, similar to previously reported on same population[37], while 12.5 in 100,000 point prevalence was reported for nDNA mutations affected patients. They also reported a minimum point prevalence of 10.7 in 100,000 at-risk healthy individuals, both children and adults. Total prevalence estimates in Canada[40] for paediatrics and adults reported even a higher estimate of 1 in 3989 clinically affected patients. In Japan, an early study[41] on children with RC disorders caused by nDNA mutations estimated 10 in 100,000 showing neonatal onset phenotypes. Recent extensive nationwide cohort of general Japanese population revealed a 2.9 in 100,000 prevalence[42]. Frequency of MDs was varied among prefectures as the highest prevalence of 8.4 in 100,000 seen in Kagoshima, although genetic background of the Japanese population is thought to be homogeneous. Many factors drove observed variations of MD frequency. First is the geographical element and genetic backgrounds of studied populations. Additionally, increased frequencies were recorded after 2004 in several studies[40,43], most likely due to introduction and availability of NGS techniques[33,44]. Many of these studies reported defects of CI are the most common enzyme defects seen in RC disorders[35–37,41] with one study reporting MT-ND5 and MT-ND6 genes as mutation hotspots[45], or the second most common following tRNA[37] or CIV[46] defects. Another important observation from general population inclusive studies is the difference in frequency of MDs caused by mtDNA and nDNA mutations between age groups, where mtDNA mutations are predominantly seen in adults and nDNA mutations are more common in children[35,36,45], similar to previously reported consensus[47,48] (Table 1).

Table 1 Prevalence of MD in literature

| Nationality | Period | Defective genome | Age demographic | Phenotype | Prevalence (in 100,000) | 95% CI | Cohort size | Ref. |
|---|---|---|---|---|---|---|---|---|
| Northeast England | 1990-2004 | mtDNA | Adults >16 years | Clinically affected | 9.18 | 7.8-10.8 | 141 | [37] |
| | | | Children and adults | At-risk | 16.5 | 14.8-18.3 | 332 | |
| Northeast England | 1990-2011 | Total | Adults >16 years | Clinically affected | 23 | 14.6-34.5 | 266 | [39] |
| | | nDNA | | Clinically affected | 2.9 | 2.2-3.7 | 62 | |
| | | mtDNA | | Clinically affected | 9.6 | 8.3-11 | 204 | |
| | | mtDNA | Children and adults | At-risk | 10.7 | 9.6-12.2 | 282 | |
| North Cumbria - England | n/a | mtDNA | Live births | Clinically affected, at-risk | 540 | 300-890 | 3168 | [38] |
| Southeastern Australia | 1987-1996 | Total | Children | Clinically affected | 5 | 4-6.2 | 86 | [36] |
| Centro region of Portugal | 1997-2006 | Total | Children | Clinically affected | 1.5 | 0.89-2.1 | 78 | [46] |
| France | 3-year span | Rare mtDNA | Children and adults | Clinically affected | 7.4% of total RC | n/a | 743 | [45] |
| | | | Neonates | Clinically affected | 10 | n/a | | |
| Japan | 2007-2013 | Total | | | | | 232 | [41] |
| Japan | 2018-2019 | Total | Children and adults | Clinically affected | 2.9 | 2.8-3 | 3629 | [42] |
| Spain | 2014-2020 | Total | Children and adults | Clinically affected | 2.3 | 2.14-2.47 | 2761 | [43] |
| | | | Children | Clinically affected | 6.34 | 5.71-6.97 | 751 | |
| | | | Adults | Clinically affected | 1.36 | 1.22-1.5 | 837 | |
| Canada | 1988-2019 | Total | Children and adults | Clinically affected | 25.1 | n/a | 3123 | [40] |

## Treatment and current therapies

Due to the lack of genotype-phenotype correlation and the complex heterogeneity, there are no therapies or standardize treatment plans so far for MDs. However, symptoms are managed by practices aimed to enhance mitochondrial function or energy production. Most commonly are dietary supplements such as electron acceptors, including Coenzyme Q10 (CoQ10), antioxidants, including vitamins E and C, and creatine[49,50] as an alternative source of Energy. Studies on the use of supplements offer no real evidence supporting they are effective, and often lack uniformity and set parameters[51]. Tailored dietary monitoring and adopting diets like ketogenic diet, high-nitrate diet, and low-residue diet are also under consideration[51–53]. Equally limited by lack of evidence, no studies on humans, and no studies on patients. Gene editing technologies and gene therapies are being proposed as alternatives for more potent treatments. The most controversial is mitochondrial replacement therapy (MRT), aimed at replacing defective mitochondria from carrier mother by healthy mitochondria from donor oocyte[54]. Aside from being only useful with defective mtDNA, numerous safety[55] and ethical considerations have hindered MRT adaption, resulting in only a handful clinically translated procedures[54]. Other tools like CRISPR/Cas9, endonucleases, and recently the RNA-free base editor[56] are currently investigated for correction of pathogenic mutations, and showed success in murine models[57,58]. However, limitations arise from the difficulties in successful delivery of editing systems into the mitochondria and possible off-target effects[59].

## Mitochondrial maintenance and quality control in stress and disease

Several proteins exist in the mitochondrial matrix for mtDNA maintenance, including DNA polymerase gamma (POLG) important for replication and proofreading, important mitochondrial transcription machinery member transcription factor A of mitochondria (TFAM) that is also a major component of the mitochondrial nucleoid, along with other nucleoid associated proteins such as mtDNA helicase Twinkle important for unwinding double stranded DNA during replication, and mtDNA single-stranded DNA-binding protein (mtSSB) important for single strand DNA stabilization[60]. Errors arising from faulty maintenance can cause mtDNA mutations, and therefore compromise function and OXPHOS. Reactive oxygen species (ROS) are another source of mtDNA mutations. ROS are by-products of the ETC and have important function in mitochondrial signalling under a certain threshold maintained by several enzymes acting as antioxidants[61]. Accumulation of ROS leads to mtDNA oxidative-damage, in addition to damaging proteins and lipids[62]. Although mtDNA is surrounded by nucleoid proteins, they are not as protective as nDNA histone proteins and do not adequately protect it from ROS-induced damage. Repair is also less efficient than nDNA repair mechanisms, rendering mtDNA more prone to mutations[63]. Compromised OXPHOS generates mitochondrial stress that is relayed to the nucleus by

signals, including ROS increase or ATP levels decrease, causing activation of one or several stress response pathways depending on the type and duration of signals[13].

## Repair of mtDNA

To avoid accumulation of mtDNA mutations, POLG also participates in proofreading after replication. POLG able to participate in replication but lacking proofreading function led to mice, also called mutator mice, to develop multi-systemic disease and premature aging[64]. Mutations remaining after replication, arising from errors in homeostasis and those from oxidative damage will be subjected to repair, protecting mitochondria from accumulating mutations and activating more drastic responses. Repair system of mtDNA is composed of many proteins, all of which encoded by nuclear genome, and act similarly to those involved in nDNA repair[65]. Several mtDNA repair processes, including base excision repair, single-strand break repair, mismatch repair, and possibly homologous recombination, have been identified[65].

## Mitochondrial biogenesis

Regulating number of mitochondria to match energy levels and demands is critical for quality control and homeostasis in cells. The most important player and the master regulator of modulating mitochondrial number and biogenesis is the transcriptional co-activator peroxisome proliferator-activated receptor gamma coactivator-1 alpha (PGC1a)[66]. Induction of PGC1a was first identified in brown adipose tissue (BAT) in response to cold temperatures, ultimately increasing thermogenesis[66]. Increased level of glucagon during fasting also induces PGC1a expression in liver, upregulating gluconeogenesis[67]. PGC1a interacts with other coactivators or transcription factors like the activator protein-1 (AP1) family to recruit other regulators like CRE-binding protein (CREB), and recruitment of mediator complex. In addition, it regulates activity of number of transcription factors like peroxisome proliferator-activated receptor gamma and alpha (PPARg, PPARa), estrogen receptor-related alpha (ERRa), nuclear respiratory factor 1 (NRF1), hepatocyte nuclear factor 4 alpha (HNF4a), and forkhead box O1 (FoxO1)[68,69]. Therefore, promoting response to metabolic changes and metabolic stresses.

## Mitochondrial dynamics

Normal cellular function requires high levels of mitochondrial fitness, regulated by processes of fusion and fission. These processes are regulated by proteolysis and post-translational modification and mediated by GTPases proteins of the dynamin family[70,71]. Fission is mediated by dynamin-related protein (Drp1) located in the cytosol and recruited by mitochondrial membrane proteins like Fis1 (mitochondrial fission 1 protein), Mff (mitochondrial fission factor), MiD49 (mitochondrial dynamics protein of 49 KDa), and

MiD51. Drp1 inhibition causes mitochondria to elongate and collapse[72], while mutant patient who died after birth displayed malnutrition, multi-system abnormalities and optic atrophy[73]. Fusion is mediated by three main GTPases, the IMM optic atrophy protein 1 (Opa1), and OMM mitofusins Mfn1 and Mfn2. Fusion proteins have been found to also be important for mtDNA stability[74], and deficiency cause a wide range of clinical phenotypes such as optic atrophy (Opa1 deficient), myopathies, neuropathies, and ataxia. Absolutely essential for development, survival, growing and dividing, but also required under cellular stress conditions of a certain degree[70,71]. Oxidative stress, starvation, UV-radiation, mtDNA mutations, or even changes in metabolism can regulate mitochondrial dynamics and switch to a more hyper-fused state or a more fragmented state. For example, mitochondrial fusion can compensate the effect of mutant mitochondria in heteroplasmic cells by the exchange of functional components from a wild-type mitochondria like proteins and lipids, enhancing OXPHOS[70,71]. One response to stress, aimed at increasing ATP production, is the elongation of mitochondria by increasing fusion thus promoting survival, called stress-induced mitochondrial hyperfusion (SIMH)[75]. Another is the elongation of mitochondria by inhibiting fission and escaping autophagy under starvation stress[76].

## Mitophagy

Mitochondrial biogenesis and dynamics are also linked to the selective clearance of damaged mitochondria that incur persistent mutations that cannot be corrected, as well as the reduction in mitochondrial number in cells undergoing metabolic shifts, a process known as mitophagy[77]. Post-translational modification of Atg32 by casein kinase 2 (CK2) and Mitogen-activated protein kinase Hog1 regulates mitophagy in yeast, allowing Atg32 to interact with Atg11[78]. Dnm1, a DRP1 homolog, recruits Atg11 to mediate mitochondrial fragmentation. Atg32, Atg8, and Atg11 interact together and form a complex that governs mitochondrial dynamics and mitophagy initiation. Mitophagy in mammals is mediated by two pathways, the first of which is activated by numerous receptors and adapters such as BNIP3 and NIX, FUNDC1, BCL2L13, and FKBP8[77]. The alternative mechanism is mediated by PINK1-Parkin-driven ubiquitination of the OMM of damaged mitochondria. The latter mechanism induces fission of defective mitochondria via PINK1 indirect stimulation of DRP1[79], hence aiding in energy homeostasis and maintenance. Several conditions dramatically promote mitophagy via distinct mechanisms. For example, dissipation of mitochondrial membrane potential and inflammation induce the PINK1-Parkin pathway[80,81], whereas starvation and hypoxia induce mitophagy via the receptor-mediated pathway[78,82].

## Apoptosis

Cells respond to numerous stimuli from either outside or inside the cells, many of which cause prolonged or irreversible damage that cannot be regulated, requiring cells to commit to programmed cell death. Apoptosis is triggered by the activation of initiator caspases 3 and 7, which are activated via two different mechanisms[83]. The first is the extrinsic pathway,

in which signals bind to death receptors on the membrane, activating caspase 8, which then activates initiator caspases[84]. Intrinsic signals, such as DNA damage, trigger the intrinsic pathway, also known as the mitochondrial pathway of apoptosis. Mitochondrial proteins, such as cytochrome c, are released into the cytosol during mitochondrial outer membrane permeabilization (MOMP)[85,86], resulting in the formation of the apoptosome complex[87], which consists of released proteins and apoptotic peptidase activating factor 1 (APAF1)[88]. By activating caspase 9, apoptosomes eventually activate initiator caspases.

## Mitochondrial Unfolded Protein Response

Protein misfolding in the endoplasmic reticulum (ER) causes their accumulation in the ER lumen and sends a signal to the nucleus, activating the transcription of chaperones and phospholipid biosynthesis enzymes. The activated signalling pathway is a well-documented cellular response to proteotoxic stress in yeast and mammalian cells, and it is known as the unfolded protein response (UPR)[89]. Proteotoxic stress has also been shown to activate a specific stress response mechanism in mitochondria. First described in mammalian cells, unfolded aggregates of ornithine transcarbamylase (OCT) in mitochondrial matrix signals nuclear gene expression of mitochondrial chaperones such as chaperonin 60, chaperonin 10 (Cpn60, Cpn10), and mitochondrial isoform of DnaJ, and proteases like caseinolytic mitochondrial matrix peptidase proteolytic subunit (CLPP)[90]. Severe oxidative stress resulting from complete lack of mtDNA also promoted expression of mitochondrial chaperones Cpn60 and Cpn10 (Selective induction of mitochondrial chaperones). Central players in the regulation of mitochondrial UPR ($UPR^{mt}$) were identified to be stress activated transcription factor (AtfS-1) in *C. elegans* and activating transcription factor 5 (Atf5) in mammals. In *C. elegans*[91], AtfS-1 was shown to be continuously imported into the mitochondria and rapidly degraded under normal conditions. Under proteotoxic stress induced by impairing mitochondrial proteases, or treatment with ethidium bromide, the $UPR^{mt}$ is activated by AtfS-1. AtfS-1 accumulates in the cytosol and translocates to the nucleus. There it was shown to activate a transcriptional profile including mitochondrial chaperones, other stress induced transcription factors, genes involved in glycolysis, and even components of mitochondrial import system. AtfS-1 requires functional mitochondrial targeting sequence (MTS) to regulate homeostasis and nuclear localization sequence (NLS) for stress-induced $UPR^{mt}$. It was also suggested that AtfS-1 promotes ATP production during oxidative stress, by positively modulating glycolysis and negatively regulating TCA and OXPHOS transcripts[92]. Another transcription factor from the ATF family, Atf5, was sufficient to induce $UPR^{mt}$ in *C. elegans* lacking AtfS-1 during proteotoxic stress[93]. Oxidative stress in mammalian cells induced transcripts of Atf5 and inhibiting ETC complexes and/or inhibiting mitochondrial membrane potential, induced expression of chaperones and proteases in Atf5-dependent $UPR^{mt}$ activation. Atf5 was shown to have mitochondrial maintenance properties in HEK293T cells under basal conditions, and knockdown of *Atf5* under cellular stress impaired cellular proliferation. Furthermore, phosphorylation of the eukaryotic translation initiation factor 2A (eIF2a) increased Atf5 synthesis[93], highlighting, with several other studies[94,95], a link between $UPR^{mt}$ with a general adaptive pathway activated by plethora of stress signals called the mitochondrial integrated stress response ($ISR^{mt}$).

## Mitochondrial Integrated Stress Response

The core of ISR$^{mt}$ response is phosphorylation and activation of eIF2a, leading to a global decrease of cellular translation but selective induction of a set of effector transcription factors[96]. The main and perhaps the best characterized is another member of the ATF family, activating transcription factor 4 (Atf4), in addition to DNA damage inducible transcript 3 (DDIT3, also known as CHOP) and Atf5. To initiate ISR$^{mt}$ response, Atf4 acts on a range of downstream target genes[96], including genes involved in serine synthesis one of which is phosphoglycerate dehydrogenase (PHGDH), others are one-carbon metabolism including MTHFD2 (methenyltetrahydrofolate cyclohydrolase), and hormone secretion like GDF15 (growth differentiation factor 15) and FGF21 (fibroblast growth factor) that promotes fatty acid oxidation[97]. Many sources of stress can activate the ISR$^{mt}$[98,99], facilitated by four different eIF2a kinases acting as stress sensors. Perhaps the two most recognized pathways for mitochondrial stress induced ISR$^{mt}$ activation are mediated by general control nonderepressible 2 (GCN2) and heme regulated inhibitor (HRI) eIF2a kinases. Impaired ETC and decrease in aspartate and asparagine cellular levels activate ISR$^{mt}$ by activating GCN2[98]. ETC dysfunction and a decrease in membrane potential also activate an IMM metallopeptidase OMA1, that cleaves OPA1 inducing mitochondrial fragmentation and cleaves another IMM protein DELE1 (DAP3 binding cell death enhancer 1)[100], that translocates to the cytosol and activates HRI. OMA1 is also activated by ETC inhibitors that increase membrane potential[101]. Although the protein kinase R-like ER kinase (PERK) is ER restricted, it was described in the ROS-induced mitochondrial stress activation of ISR$^{mt}$. The fourth kinase, protein kinase R (PRK) is activated during viral infections by binding to double stranded RNAs.

Many research investigating global responses elicited by mitochondrial abnormalities and ETC dysfunctions in mitochondrial disease models have also demonstrated activation of ISR$^{mt}$ pathway and its role in adaptability or disease progression[102–105]. ISR$^{mt}$ was activated in a MD animal model of Twinkle mutation, or Deletor mouse, demonstrating mitochondrial myopathies (MM), but showed temporal progression in successive phases[99]. FGF21, which was active in the early stages and modulated glucose intake and metabolic regulation, as well as GDF15 and Mthfd2, promoted phenotype progression. Later phase revealed that Atf5 but not Atf4 was upregulated, and the last stage revealed a minor increase of Atf3, yet another member of the ATF family. A similar ISR$^{mt}$ gene profile was found in the muscles of Twinkle mutation patients. Actinonin inhibition, on the other hand, induced Atf3, Atf4, and Atf5 at later phases of ISR$^{mt}$ in mouse myoblast cells. It also exhibited an increase in OPA1 and heat shock proteins, which were not detected in Deletor mice or human patients, demonstrating the complexity of stress responses between organisms and cell types. While this study clearly demonstrated that ISR$^{mt}$ has a negative effect on the severity and progression of MM caused by mtDNA defects, it did not conclude direct drivers of the phenotype. Role of FGF21 as a mediator in the signalling cascade that further facilitates disease progression or as a main effector was not resolved. In another OXPHOS deficient mouse model exhibiting cardiomyopathy, activation of ISR$^{mt}$ in the heart served a protective role[102]. Cardiac-specific Cox10, a nuclear encoded CIV subunit, mutant animal with early-onset fatal cardiomyopathy activated ISR$^{mt}$ via the OMA1-DELE-HRI signalling

cascade, and upregulated effector Atf4, which upregulated ISR target genes. The loss of OMA1 or DELE1 in Cox10 knockouts exacerbated the cardiomyopathy phenotype, reduced lifespan, and enhanced ferroptosis-mediated cell death. Given the early disease onset of COX10 knockout mouse, it is difficult to determine if this $ISR^{mt}$ activation represents an end stage adaptation mechanism to the aggravated phenotype or a much earlier response to OXPHOS deficit. It also raises the question of whether there were early adaptive mechanisms aimed at restoring homeostasis prior to complete tissue failure and $ISR^{mt}$ activation. Previously reported cell and tissue variability[98,99] was not demonstrated here; nonetheless, cellular variations in the heart during OXPHOS deficiency-induced cardiomyopathy may exist.

It remains debatable whether $ISR^{mt}$ activation in response to metabolic stress plays a protective role or is a driver of disease progression, especially in OXPHOS deficiencies resulting from different ETC complexes. CI defects are one of the most common and most frequent in MDs, yet current state of their characterization is underwhelming. The first CI model was Ndufs4, an accessory subunit important for assembly, knockout mice which demonstrated a neurodegenerative pathology akin to Leigh syndrome-like in humans[106]. Although ATP and glucose levels were not significantly altered, knockout mice's motor function and weight began to decline after only 35 days, and they only survived for up to 50 days. Neuron and glia specific *Ndufs4* knockout mice[107] exhibited a phenotype comparable to systemic knockouts, including early manifestation and a short life span.

Gene-trap knockdown of another CI assembly subunit, Ndufs6, caused heart-specific CI deficiency and OXPHOS deficit[108]. $Ndufs6^{gt/gt}$ mice showed cardiac enlargement, weight loss, cardiac fibrosis, and heart failure. However, phenotypes did not emerge until 4 months in male mice and 8 months in female mice, while younger mice had no overt phenotype and were phenotypically normal. This model is ideal for determining how mitochondrial dysfunctions influence disease outcomes and allows us to trace cellular intrinsic regulation of energy homeostasis within a tissue as well as early to late responses to failing adaptations.

## Statements and questions

Mitochondrial OXPHOS is a tightly regulated process which activates endogenous adaptation mechanisms if there is dysfunction. These protective machineries are diverse, and no single factor has been assigned as a central player in mitochondrial or metabolic disorders. These mechanisms fail to persist or lead to detrimental effects on tissues if source of dysfunction prevails. This in turn leads to an irreversible tissue failure. CI dysfunction, especially in the context of cardiomyopathy, has not been studied and the underlying mechanisms involved in the pathogenesis are not well understood.

Due to the limitation of earlier works in literature, the following questions arise:

1. What factors contribute to the insufficiency of these endogenous adaptive machineries?

2. Is there a point of no return in which cells switch to maladaptive state?

3. How are these mechanisms modulated by different cell types of the myocardium?

## Aim and objectives

The main aim of this project is to comprehensively understand the pathogenesis of mitochondrial CI dysfunction leading to tissue failure, for the purpose of identifying suitable therapeutic targets.

I proposed three key objectives in this study to address the collective goal:

1. To trace the adaptive machinery in response to metabolic dysfunction from adaptation to malfunction in the heart.

2. Identify cell fate determinants responsible for transitioning.

3. Characterize differences of cell responses to same stressors.

# Materials and methods

## Materials

**Table 2 Antibodies used in immunostaining**

| ANTIBODY | SOURCE | IDENTIFIER |
|---|---|---|
| **Rabbit monoclonal Anti-Atf3** | Abcam | ab254268 |
| **Rat monoclonal Anti-CD68** | BioLegend | 137001 |
| **Rabbit polyclonal Anti-GFP pAb-HRP-DirecT** | MBL | 598-7 |
| **Goat pAb to Rb IgG (Alexa Fluor 555)** | Abcam | Ab150078 |
| **Rabbit polyclonal Anti-PGC1a(N-terminal)** | Abcam | Ab191838 |
| **Goat polyclonal Anti-cTnnI3** | Abcam | Ab56357 |
| **Donkey anti-Goat IgG (H+L) Cross-Adsorbed (Alexa Fluor 488)** | ThermoFisher | A-11055 |

**Table 3 Probes used in ddPCR**

| PROBE | UNIQUE ASSAY ID |
|---|---|
| **Atf3, Mmu** | qmmucip0035769 |
| **Atf4, Mmu** | qMmuCEP0056683 |
| **Atf5, Mmu** | qMmuCIP0029332 |
| **Atf6, Mmu** | qMmuCEP0053948 |
| **Il6, Mmu** | qMmuCEP0054186 |
| **Tbp, Mmu** | qmmucip0042759 |

**Table 4 Software and algorithms used in analysis**

| SOFTWARE | VERSION | SOURCE | IDENTIFIER |
|---|---|---|---|
| **Python** | v3.8.5 | [109] | http://www.python.org |
| **ScanPY** | v1.6.1 | [110] | https://github.com/scverse/scanpy |
| **PAGA** | v1.2 | [111] | https://github.com/theislab/paga |
| **ComBat** | v0.3.0 | [112] | https://github.com/brentp/combat.py |
| **Cell Ranger** | v4.0.0 | | https://support.10xgenomics.com/single-cell-gene-expression/software/pipelines/4.0/what-is-cell-ranger |
| **Prism** | v8 | | www.graphpad.com |
| **EnrichR** | March 29th, 2021 | [113,114] | https://maayanlab.cloud/Enrichr/ |
| **iDEP** | v0.96 | [115] | http://bioinformatics.sdstate.edu/idep96/ |
| **TRRUST** | v2 | [115] | https://www.grnpedia.org/trrust/ |
| **ReprogrammingRecovery** | | [116] | https://github.com/gifford-lab/ReprogrammingRecovery |
| **Matplotlib** | v3.4 | [117] | https://matplotlib.org/ |
| **UMAP** | v3 | [118] | https://github.com/lmcinnes/umap |
| **Leiden** | v3 | [119] | https://github.com/vtraag/leidenalg |
| **ForceAtlas2 (FA)** | v3 | [120] | https://github.com/bhargavchippada/forceatlas2 |
| **HISAT2** | v2.1.0 | [121] | http://daehwankimlab.github.io/hisat2/ |

# Methods

## Animal models

*Ndufs6*$^{gt/gt}$ heterozygous mouse sperm of mixed genetic background, C57BL/6J and 129/Ola, was kindly provided by Dr. David Thorburn. All experiments concerning animal use were conducted in accordance with National Cardiovascular and Cerebral Center guidelines. No randomization, sample size estimation, or blinding was done.

## Echocardiography

Prior to echocardiography, mice were anesthetized using 0.5-1.0% isoflurane administered via a mask covering the nose and mouth of the animals. Transthoracic echocardiography was performed on unconscious mice with a Vevo 3100 imaging system (Visualsonics, Inc.). M-mode echocardiographic images were obtained from a short-axis view to measure the left ventricular ejection fraction (LVEF).

## Immunohistology

### Fresh-frozen sections

Freshly dissected heart tissue was embedded in OCT compound (Sakura Finetek) after ice-cold PBS perfusion and was frozen by incubating on isopentane chilled in liquid nitrogen. Tissue blocks were stored at −80 °C until sectioning. Prior Sectioning, tissue blocks were allowed to equilibrate at −20 °C for at least 2 h then were cut at 8 μm thickness (Leica biosystems) on adhesive glass slides (Matsunami) and stored at −80 °C for downstream histological analysis. Sections were fixed with Acetone for 10 min at -20 °C, followed by blocking with Blocking One Histo (Nacalai) for 10 min at room temperature. Primary antibodies anti-Atf3 (1:1000, Abcam), anti-CD45 (1:500, BioLegend) and anti-CD68 (1:500, BioLegend) incubated at 4 °C overnight, followed by 1 h incubation of secondary antibodies anti-rabbit (1:500 Invitrogen) and anti-rat (1:500 Invitrogen), were used to detect the expression of Atf3 and evaluate immune infiltration. Hoechst 33342 (1:1000, DOJINDO) was used for nuclear visualization. Images were obtained using confocal laser scanning microscope (Olympus, FV3000) for observation and all-in-one microscope (Keyence, BZ-X810) for signal count and analysis. Signal was quantified as area percentage using BZ-X800 Analyzer software.

### Fixed-frozen sections

Freshly dissected heart tissue was immersed in ice-cold 4% Paraformaldehyde Phosphate Buffer Solution (4% PFA, WAKO) after 4% PFA perfusion for 24 h followed by serial immersion of the tissue in 10%, 20%, 30% sucrose in PBS for 24 h each or until the tissue sank to the bottom. Tissue was embedded in OCT compound (Sakura Finetek) and was frozen by chilling in at −80 °C. Tissue blocks were stored at −80 °C until sectioning. Prior Sectioning, tissue blocks were allowed to equilibrate at −20 °C for at least 2 h then were cut at 8 μm thickness (Leica biosystems) on adhesive glass slides (Matsunami) and stored at −80 °C for downstream histological analysis. Sections were air-dried for at least 30 min. For antigen retrieval, sections were submerged in 1X Citrate buffer, pH 6.0 (Abcam) and microwaved for 2 min followed by 10 min boiling in -98 °C water bath. Sections cooled for at least 30 min at room temperature were submerged under running hot water for 1 min and washed with 1X buffer two times for 3 min. Protocol was continued as described using primary antibodies and anti-cTnnI3 (1:500, Abcam) anti-Atf3 (1:500, Abcam) incubated 4 °C for 1 and 2 overnights respectively.

### ZENON double staining

Protocol for double staining with two rabbit antibodies was performed as described for fresh-frozen tissue. Sections were first stained with primary antibody anti-Atf3 (1:500, Abcam) incubated at 4 °C two overnights, followed by 1 h incubation of secondary antibody anti-rabbit (1:500 Invitrogen). Anti-Pgc1a (1 μg, Abcam) was labelled with Zenon Rabbit IgG Alexa Fluor 555 (ThermoFisher) just before incubating at 4 °C two overnights. Images were obtained using confocal laser scanning microscope (Olympus, FV3000), and nuclei count was performed manually on 3 samples and 5 sections.

## Nuclei preparation

### Nuclei isolation from heart tissues

Nuclei were isolated according to Frankenstein protocol[122] with minor modifications. All samples, reagents and steps were kept and performed on ice. Heart tissue was cut into small pieces in 0.5 ml ice-cold EZ PREP lysis buffer (Sigma) and homogenized using 2 ml glass douncer (8 times with pastel A and 1 time with pastel B) and incubated on ice with additional 1 ml ice-cold EZ PREP lysis buffer for 3 min with gentle mixing using a wide bore tip two times. Homogenate was filtered through a 70 μm followed by 20 μm cell strainer (PluriSelect) and centrifuged at 500 x g for 5 min at 4 °C to remove cell debris and aggregates. Nuclei pellet was suspended in another 1.5 ml ice-cold EZ PREP lysis buffer and incubated on ice for 3 min. After

centrifugation at 500 x g for 5 min at 4 °C, nuclei pellet was incubated with nuclei washing and resuspension buffer consisting of 1X PBS, 1% BSA, 0.1% Tween-20 and 0.2 U/µl RNase inhibitor (TAKARA Bio) for 5 min before resuspension with additional 1 ml. Nuclei were centrifuged at 500 x g for 5 min at 4 °C and the nuclei pellet was resuspended with 0.5 ml nuclei washing and resuspension buffer containing DAPI stain (DOJINDO) for nuclei labeling. Final nuclei count was determined by counting nuclei with a hemocytometer (NanoEntek) under fluorescent microscope (Keyence BZ-X810).

### Nuclei sorting

Isolated nuclei, kept on ice, were immediately sorted by Fluorescence Activated Cell Sorting using FACS Aria Fusion cell sorter (Becton Dickinson, National Cerebral and Cardiovascular center) into 15 ml tubes containing 7 ml bed nuclei washing and resuspension buffer not containing Tween-20; for complete removal of detergent. The 355 nm ultraviolet laser was used for analysis and nuclei sorting, while scattering detection of 488 nm blue laser was used to record forward-scatter characteristics (FSC) and side-scatter characteristics (SSC). Samples' data were recorded and analyzed for gating and single nuclei selection using BD FACS DIVA 8.0.3 software. Sorted nuclei population was determined by two pre-gated parameters. The first gating was set by DAPI area (DAPI-A) against count to remove debris and aggregation, then homogeneous signal peak was selected for the second gating. Second gating was set by trigger channels FSC area (FSC-A) against DAPI-A; selecting signal threshold falling between 50-150 (x1000) FSC-A and 100-150 (x1000) DAPI-A. Samples were injected into the stream using 70-micron nozzle achieving high sheath pressure (70 psi). On average, sample run time was 15 min and efficiency rate were higher than 95%. Sample was then centrifuged at 500 x g for 10 min at 4 °C and pellet was resuspended with nuclei washing and resuspension buffer not containing Tween-20, to a final concentration of 1000 nuclei/µl. Final nuclei count was determined by counting nuclei with a hemocytometer (NanoEntek) using all-in-one microscope (Keyence, BZ-X810).

## Single cell transcriptomics

### Library preparation and sequencing

Droplets capturing single nucleus from whole heart nuclei suspension were used for library generation in the 10X Genomics Chromium controller according to the manufacturer's instructions in the Chromium Single Cell 3′ Reagent Kit v.3 User Guide. Additional components used for library preparation include the Chromium Single Cell 3′ Library and Gel Bead Kit v.3 (PN-1000092). Libraries were prepared according to the manufacturer's instructions using the Chromium Single Cell 3′

Library and Gel Bead Kit v.3 (PN-1000092) and Chromium i7 Multiplex Kit (PN-120262). Final libraries were sequenced on Illumina. All libraries were sequenced to a depth of at least 20,000 total mean reads per nucleus.

## Raw sequencing reads processing

Cell Ranger v.5.0.0 pipeline provided by 10X Genomics was used to process raw sequencing reads. Reads were aligned to mouse mm10 genome. Gene-barcode matrices were created by quantifying UMI counts per gene per cell and the data were aggregated and normalized creating a combined gene-barcode matrix. Individual matrices of samples were used for downstream processing and analysis.

## Gene matrix pre-processing, filtering, and cell clustering

Python Scanpy package v1.6.1 was used for further pre-processing, filtering, and clustering of gene matrices obtained by Cell Ranger. Gene matrix was first converted to a well-constructed dataframe in the form of an anndata object. Poor quality cells were removed by filtering out cells (sc.pp.filter_cells command) based on number of counts and mitochondrial genes percentage. Cells with fewer than 200 and greater than 3000 genes and cells with higher than 0.5% mitochondrial genes were excluded. Genes expressed in less than three cells were considered outliers and were excluded by filtering in the pre-processing step. To allow counts to become comparable among all cells, library-size was corrected by normalizing (sc.pp.normalize_total command) to a scale factor of 10,000, followed by log-transformation (sc.pp.log1p command) and scaling (sc.pp.scale command) the data to follow a linear-regression model. Dimensionality reduction was computed using linear principal component analysis (sc.tl.pca command) and number of significant principle components (PC) to be used for clustering were determined by plotting each PC's variance ratio. Next, selected PCs were used to calculate neighbourhood graph (sc.pp.neighbors command) that is automatically embedded to compute uniform manifold approximation and projection (UMAP) graph (sc.tl.umap command) for two dimensional visualization of cells. Communities of cells were detected by Leiden algorithm (sc.tl.leiden command) with the default resolution of 1. Number of clusters obtained varied by sample and represented major cardiac cell types.

## Differential gene expression analysis and annotations

To identify highly expressed genes in Leiden clusters, differentially expressed genes were ranked (sc.tl.rank_genes_groups) using Wilcoxon rank-sum test. Genes were ranked by log2 fold change values and *p*-values. Top statistically significant

genes were used for Cell types manual annotation based on the expression of cell-specific marker genes manually curated from literature.

## ComBat integration

For comparison between two or more datasets, ComBat algorithm was used for batch effect correction. Data matrices were first converted to anndata objects where each dataset was annotated under a new observation column "sample", followed by merging (concatenate command) where the anndata object was then processed following previous workflow. ComBat algorithm was then used (sc.pp.combat command) to remove batch variation between samples, and significant PC's were selected to calculate neighbourhood graph and UMAP topology. Leiden clustering showed 23 clusters representing cell types previously identified in individual datasets. Differential gene expression analysis between different samples was then performed using Wilcoxon rank-sum test and genes were ranked by log2 fold change values and *p*-values. Ranked genes lists were used for comparative analysis and downstream gene ontology analysis.

## Sub-clustering

Integrated WT, *Ndufs6*$^{gt/gt}$ 8 weeks, *Ndufs6*$^{gt/gt}$ 17 weeks cardiomyocytes sub-clusters 3, 6, 8, 9, 11 and 17 were isolated and reclustered, UMAP graph was computed, and Leiden algorithm was used with 1 resolution. For the sake of reproducibility, sub-clustered cardiomyocytes were stored as anndata file and further analysed. Differential gene expression analysis between different samples was then performed using Wilcoxon rank-sum test and genes were ranked by log2 fold change values and *p*-values. Ranked genes lists were used for comparative analysis and downstream gene ontology analysis.

## Pseudo-time trajectory analysis

Integrated re-clustered cardiomyocytes were used for trajectory analysis. ForceAtlas2 (FA) algorithm was used to draw single-cell graph (sc.tl.draw_graph command) using the anndata object previously calculated PCA space and neighbourhood graph. To denoise the graph, diffusion maps were computed (sc.tl.diffmap command) using the first 15 components and neighbourhood distances were calculated between diffusion components (sc.pp.neighbors command) to draw graph on the diffusion map (sc.tl.draw_graph command). Clusters were detected by Leiden algorithm (sc.tl.leiden command) with the default resolution of 1. Next, PAGA graph was calculated (sc.tl.paga command) based on embeddings connectivity maps of UMAP clusters calculated by the Leiden algorithm. The single-cell graph was

recomputed (sc.pl.draw_graph command) based on PAGA graph calculated earlier. To assign a root for pseudotime temporal path tracing, the first cluster with the highest Pgc1a expression, cluster 8, was chosen as a root.

## Gene ontology analysis

Gene lists were filtered with a *p*-value cut-off value of <0.001 and log2 fold change (log2FC) value of >1.5. GO analysis was performed on gene lists using EnrichR and *p*-values were calculated with Fisher exact test.

## RNA extraction

Freshly dissected heart tissues from PBS perfused hearts were cut into 30 mg pieces and immersed in 3X volume RNAlater (Sigma) overnight at 4 °C. Flash frozen tissues stored in liquid nitrogen were later immersed in 10X volume ice-cold RNAlater-ICE (ThermoFisher) overnight at -20 °C. Total RNA from immersed heart tissues isolated using the RNeasy Fibrous Tissue kit (Qiagen) according to manufacturer's instructions. Total RNA was converted to cDNA using High capacity cDNA Reverse Transcriptase kit (Applied biosystems) in a 20 µl reaction according to manufacturer instructions except for termination step that was set to 30 min.

## ddPCR

Droplet digital PCR was performed by using ddPCR Supermix for Probes (no dUTP) (BioRad Laboratories) and PrimePCR assay probes (BioRad Laboratories) on QX200 Droplet Digital PCR System (BioRad Laboratories) according to manufacturer's instruction. In brief, sample partitioning into droplets was performed by QX200 Droplet Generator (BioRad Laboratories) for PCR amplification followed by individual analysis of droplets on QX200 Droplet Reader (BioRad Laboratories) for absolute quantification. The level of expression was normalized to Tbp reference gene expression.

## Spatial transcriptomics

Spatial transcriptomics of Atf3-positive cells was performed using Photo-isolation chemistry (PIC) as described[123,124]. In brief, fresh-frozen tissue sections were permeabilized with HCl (Nacalai Tesque) followed by *in situ* mRNA reverse transcription using photo-caged oligodeoxynucleotides (ODNs) primers (Glen research). After first strand synthesis, anti-Atf3 antibody was used to identify region of interest (ROI) by immunostaining. UV irradiation (LED light, Prizmatix) was used for uncaging ODNs allowing in-vitro transcription reaction. Libraries were further reverse-transcribed

and paired-end sequenced on NovaSeq6000 (Illumina). Final reads were mapped to reference genome using HISAT2. Analysis was performed on the web-based integrated Differential Expression and Pathway Analysis (iDEP) tool.

## Generation of double *Atf3* KO and *Ndufs6*$^{gt/gt}$ mice with CRISPR/Cas9

CRISPR/Cas9-mediated production of KO mice was performed as described previously[125]. Briefly, Atf3 KO mice were generated by introducing gRNA/CAS9 protein solution into fertilized eggs of *Ndufs6*$^{gt/gt}$ mouse with an electroporator (NEPA21, Nepagene, Chiba, Japan). A search for gRNA and off-target sequences was performed using CRISPRdirect software (http://crispr.dbcls.jp/). Screening of the obtained mutant mice was performed by direct sequencing following PCR. The gRNAs and primers used were: 5'-ccagcgcagaggacatccga-3' for the first exon of Atf3 and 5'-cccagcagccaagagccgtt-3' for the third exon of Atf3. The genotyping primers used were: 5'-gaggtaggctgtcagaccccatgc-3' for Pr.1, 5'-gcccattctcgggtgcacactatacc-3' for Pr.2, and 5'-gccacagtggaggatgtggtccc-3' for Pr.3.

## Statistical analysis

Data were analyzed using GraphPad Prism 8 and were considered significant when $P < 0.05$. Data between two groups were compared with Student's *t*-test. Data from more than two groups were evaluated with ordinary one-way ANOVA followed by Tukey's *post hoc* analysis, and data from compound two or more groups were evaluated with two-way ANOVA followed by Tukey's *post hoc* analysis. All data are presented as mean (SD).

# Results

## Female *Ndufs6*$^{gt/gt}$ mice transitions slowly to maladaptation and has a milder phenotype

Characterization of *Ndufs6*$^{gt/gt}$ (refered to as FS6KD henceforth) mice showed discrepancies in cardiac phenotype and survival between male and female mice[108]. However, cardiac function was not thoroughly demonstrated for knockdown female mice nor younger male mice, and analysis was performed mainly on male mice 4 month of age. It was important to carefully select suitable time points that will allow us to successfully trace processes underlying transitioning, therefore, I characterized cardiac function and phenotype of FS6KD female and male mice from early age over a period of several weeks.

FS6KD mice displayed increased left ventricular systolic dysfunction with age progression indicated by a continuous decrease in left ventricle ejection fraction (EF) and increase in left ventricle internal dimension end-diastole (LVID;d)(Fig.2 a-d). However, dysfunction was exaggerated in male mice, showing reduction from 80% to 40% in EF at 8w compared to reduction to only about 60% in female mice. In addition, phenotype onset was late in female mice where EF at 18w was comparable to younger 10w male FS6KD mice (Fig.2 a, c). Echocardiography data suggested female FS6KD mice have more persistent metabolic adaptation machineries and a slower, more gradual progression to malfunction.

Cardiac injuries are known to activate inflammation, which is primarily caused by macrophage infiltration into the myocardium[126,127], and fibrosis, which is caused by activating fibroblasts into myofibroblasts and depositing extracellular matrix for tissue repair[127]. First, I performed histological assessment of 8w female FS6KD mice by Masson Trichrome (MTC) staining to examine if tissue degeneration coincides with the decrease in EF. Our findings demonstrated that FS6KD-induced metabolic dysfunction promoted the fibrosis of female mouse hearts as early as 8w (Fig.2 e).

I then stained cardiac tissues with anti-CD68 antibody, a marker for monocytes and macrophages, to assess inflammation in FS6KD mice. I found a significant increase in CD68-positive signal accumulation in FS6KD mice compared to WT (Fig.2 f-g), indicating an increase in inflammation in the myocardium. Because I observed a decrease in CD68 signal in older FS6KD tissue staining, I measured CD68-positive area in WT and FS6KD mice with age progression for quantitative analysis. Older knockdown mice did show a reduction in CD68-positive signal, resulting from a gradual decrease over several weeks rather than a steep decline (Fig.2 h).

I also observed elevated levels of *interleukin 6* (*Il6*) in FS6KD heart tissues. The trend of *Il6* expression with age progression was comparable to that of CD68 (Fig.2 i), with levels peaking in young mice and gradually decreasing over several weeks. This indicates that inflammatory signalling in the myocardium begins as early as 6w.

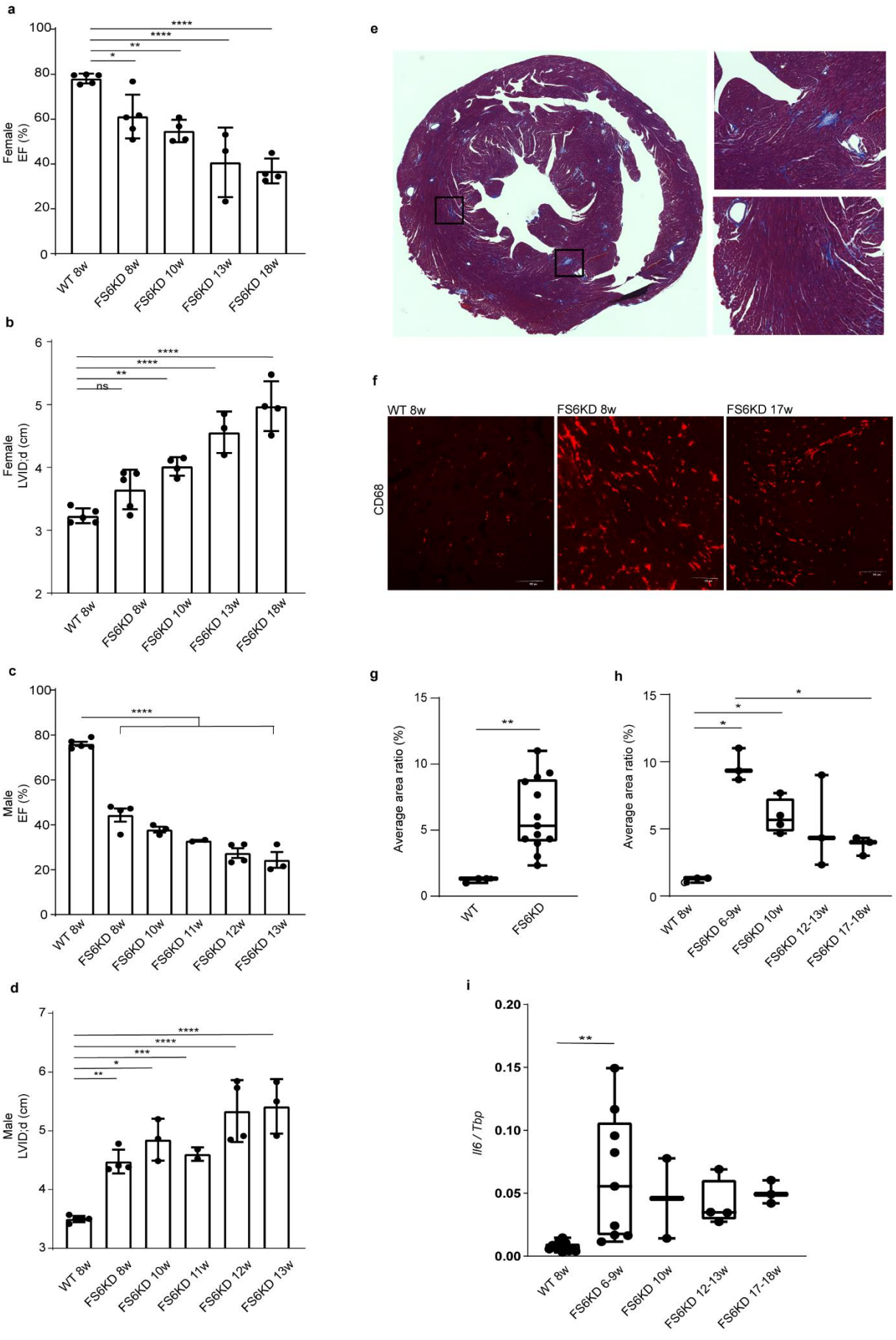
a
Female EF (%)
WT 8w
FS6KD 8w
FS6KD 10w
FS6KD 13w
FS6KD 18w
b
Female LVID;d (cm)
ns
c
Male EF (%)
FS6KD 11w
FS6KD 12w
d
Male LVID;d (cm)
e
f
WT 8w
FS6KD 8w
FS6KD 17w
CD68
g
Average area ratio (%)
WT
FS6KD
h
FS6KD 6-9w
FS6KD 12-13w
FS6KD 17-18w
i
Il6 / Tbp

**Fig 2 Assessment of female FS6KD disease progression**.

(a) Left ventricular ejection fraction of female mice (n ≥ 3). (b) Left ventricular internal diameter end diastole of female mice (n ≥ 3 per group). (c) Left ventricular ejection fraction of male mice (n ≥ 3, FS6KD 11w n = 2 per group).(d) Left ventricular internal diameter end diastole of male mice (n ≥ 3 per group, FS6KD 11w n = 2). (e) Masson's trichrome (MTC) staining of female FS6KD 8w heart tissue (x10 magnification). (f) Immunostained images of female heart tissue with CD68 antibody. Representative images from three individuals and three tissues were shown (x20 magnification). (g) Area ratio of CD68 signal in female heart tissue averaged from three tissues per n (n ≥ 3 per group). (h) Area ratio of CD68 signal in female heart tissue of different time points averaged from three tissues per n (n ≥ 3 per group). (i) Female heart tissue of different time points for *Il6* expression analyzed by ddPCR and normalized to *Tbp* expression (n ≥ 3 per group, FS6KD 10w n = 2). Significance is indicated; (a-d, h-I) one-way ANOVA followed by Tukey's post-hoc test; (g) t-test. ∗p < 0.05, ∗∗p < 0.01, ∗∗∗p < 0.001, ∗∗∗∗p < 0.0001, ns : not significant.

## Single-nucleus RNA sequencing reveals different landscapes in healthy and diseased hearts

To comprehensively identify cardiac remodelling processes under metabolic dysfunction and underline cellular-specific responses, I used single-nucleus RNA sequencing (snRNA-seq) on hearts from female WT and FS6KD mice. Using three different phenotypes: WT, FS6KD 8w showing higher EF, more adaptation, and milder phenotype, while FS6KD 17w already transitioned to severe dysfunction.

Using 10X Genomics platform, I obtained 14,593 WT nuclei, 14,102 FS6KD young (8w) nuclei, and 10,130 FS6KD older (17w) nuclei. Unsupervised clustering of individual datasets utilizing the ScanPY analytic platform resulted in the annotation of more than 20 clusters based on significant expression of cell-type specific marker genes identified by a manually curated list from the literature. The uniform manifold approximation and projection (UMAP) plot enabled the viewing of annotated cardiac cell types and sub-populations (Fig.3 a, c, e), including cardiomyocytes (*Tnnt2*, *Ttn*), fibroblasts (*Pcdh9*, *Col1a1*), endothelial cells (*Pecam1*), immune cells (*Slc9a9*, *Adgre1*), and mural cells (*Abcc9*, *Dlc1*). In addition, smaller populations such as epicardial cells (*Muc16*), endocardial cells (*Tmem108*), myoblasts (*Stox2*), adipocytes (*Car3*), and Schwann cells (*Csmd1*) have been identified (Fig.3 b, d, f).

All three datasets were comprised of all major cellular populations. I did notice a change in nuclei number comprising similar populations across datasets, like cardiomyocytes or fibroblasts, and a change in number of their sub-clusters. For example, cardiomyocytes in FS6KD 8w contained more sub-populations than FS6KD 17w (Fig.3 c, e). The variation in populations number was more evident among minor cardiac populations. I observed a reduction in epicardial and endocardial clusters in FS6KD mice compared to WT. Moreover, FS6KD mice showed diminished adipocytes population that was only found in WT. Changes in different datasets might have arisen due to technical biases introduced by microfluidics partitioning or pre-processing steps and nuclei filtering in analysis pipeline.

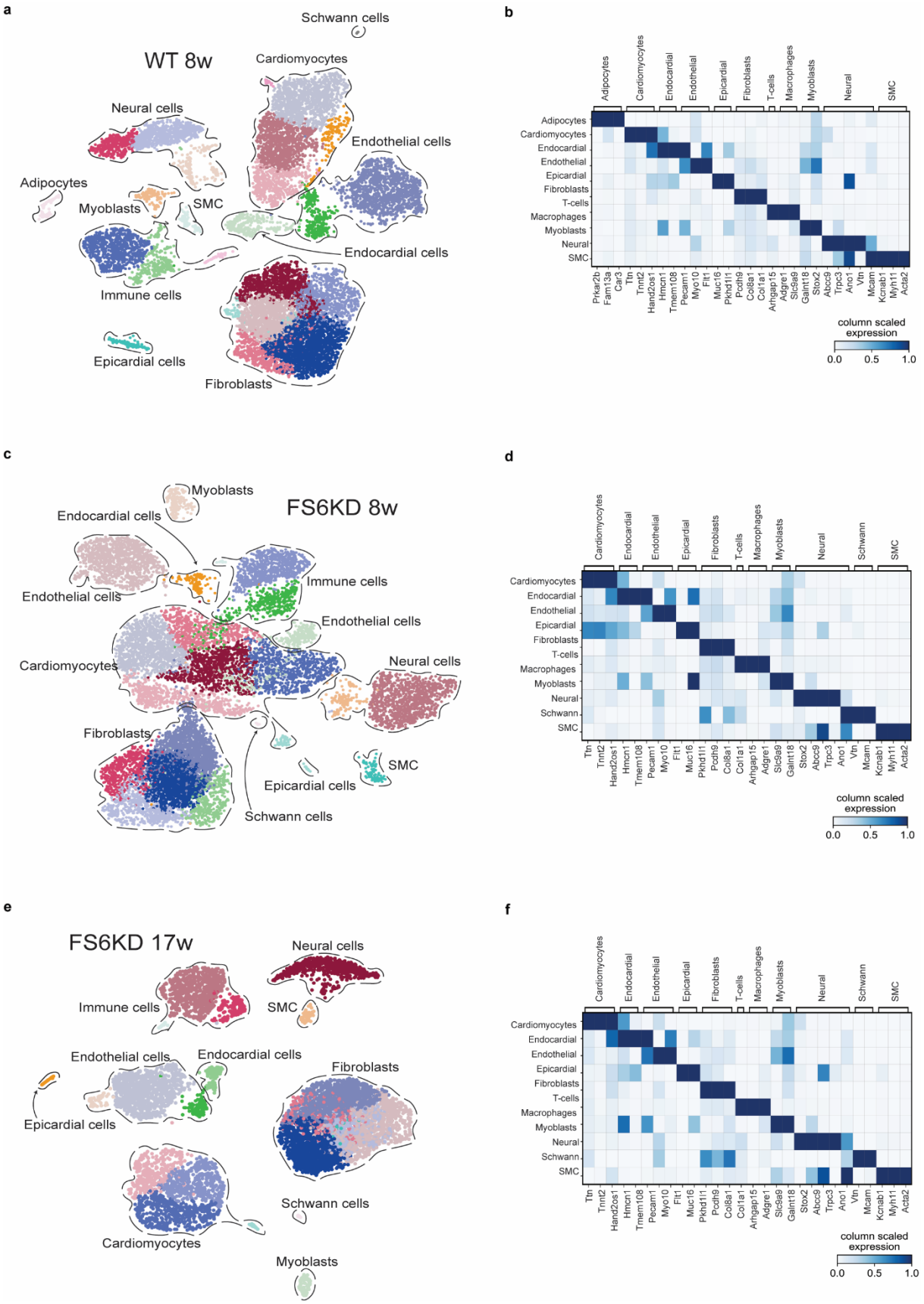


**Fig 3 Healthy vs diseases cardiac landscapes**

(a) UMAP of cardiac cellular populations of healthy WT 8w colored by leiden clusters, and (b) Heatmap of their marker genes. (c) UMAP of cardiac cellular populations of FS6KD 8w colored by leiden clusters, and (d) Heatmap of their marker genes. (e) UMAP of cardiac cellular populations of FS6KD 17w colored by leiden clusters, and (f) Heatmap of their marker genes. SMC: Smooth muscle cells.

## Cardiomyocytes are the most affected by metabolic perturbation

To avoid false interpretation of technical biases as biological variations, I performed integration on all datasets by ComBat algorithm prior to analysis. The overall landscape of cellular populations after unsupervised clustering and annotation of integrated dataset was unchanged (Fig.4 a). I evaluated the true changes in size and number of different cellular populations between datasets.

Compared to WT, percentage per dataset of cardiomyocytes population increased in young 8w heart and decreased in 17w (Fig.4 c). In contrast, I observed an opposite trend in fibroblasts population that showed a decrease in 8w but an increase in 17w.

Epicardial and endocardial populations decreased significantly compared to WT regardless of FS6KD cardiac phenotype, although slightly more decreased in 8w. Indeed, I was only able to assign adipocytes to a small population found in WT, but I could not find adipocytes populations in FS6KD. To further validate that this is not due to bias in nuclei filtering during analysis, I modified pre-processing parameters permitting larger number of nuclei for clustering, yet no additional populations were revealed.

Integration also revealed shifting in cellular states among different cell types from normal WT state (Fig.4 b). This shifting, although elicited by knockdown, was more distinguishable in 8w. Some populations like fibroblasts, endothelial cells and neural cells showed overlapping between 17w and WT.The most dramatic shift was found in cardiomyocytes populations that displayed isolated states in all three different datasets. This suggested that cardiomyocytes underwent major dynamic transcriptional reprogramming in response to metabolic dysfunction.

I compared average expression levels of *Ndufs6* between cell types in 8w FS6KD dataset. I did not observe higher knockdown in cardiomyocytes, and knockdown levels were proportional with no cell specificity (Fig.4 e). UMAP plots of *Ndufs6* expression also showed successful knockdown in all cell types in FS6KD datasets compared to WT (Fig.4 d). This result confirmed differences in state shifting between different cell types were due to actual inherent cell-type specific stress responses and not a result of variation in *Ndufs6* knockdown.

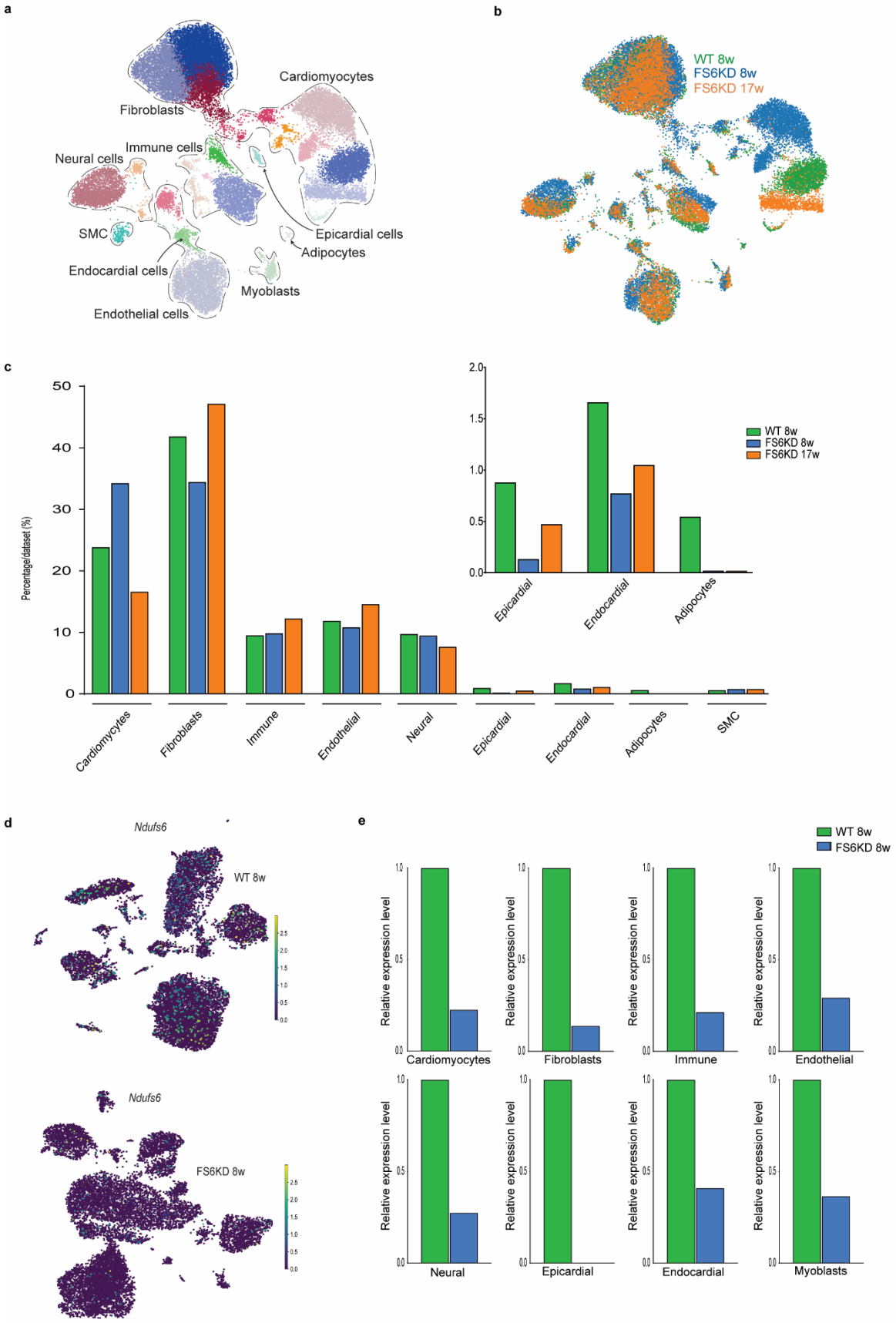


**Fig 4 Differences in cellular responses to knockdown**

ComBat integrated datasets UMAP of (a) cardiac cellular populations colored by leiden clusters, and (b) colored by dataset. (c) Cell percentages per dataset in total integrated object. (d) UMAP expression gradient of Ndufs6 in two separate datasets. (e) Relative expression levels of *Ndufs6* in cell types normalized to WT expression.

## Protective *Pgc1a* induction is downregulated in older FS6KD heart

I hypothesized that state shifting of cardiomyocytes population contained information on the transitioning from adaptation to malfunction, allowing us to investigate which machineries participate in this process. To uncover the sources of cardiomyocytes heterogeneity across different datasets, I performed unsupervised sub-clustering on isolated cardiomyocytes populations (Fig.5 a-b), DGE analysis on significant most differentially upregulated genes, and GO biological processes analysis.

Metabolic processes were the most enriched in the 8w cardiomyocytes, including those involved in maintaining glucose homeostasis and oxidative processes (Fig.5 c). Gluconeogenesis processes were upregulated as a result of energy deficit along with enrichment of fatty acid oxidation, suggesting remodelling to maintain high demand for energy expenditure. This observed metabolic switching from fatty acid oxidation to glycolysis suggested that young 8w heart is still adjusting to the decrease in energy supplies.

In the old 17w cardiomyocytes, I found enrichment in pathways involved in muscle tissue stretching and development in response to reduced cardiac output, as well as processes of response to DNA damage, stress, and cell death (Fig.5 c). There was no upregulation of metabolic pathways, implying that the myocardium had already remodelled to dysfunction due to persistent metabolic insult and failure to maintain energy homeostasis. This result was further supported by the decrease in ejection fraction and systolic dysfunction observed in previously performed echocardiography (Fig.2 a). Subsequently, I extracted DEG lists from 8w and 17w cardiomyocytes to identify participating factors involved in transitioning. *Ppargc1a* (*Pgc1a*), a transcription co-activator and master regulator of mitochondrial number and biogenesis[66]frequently increased in cells to adapt to increasing energy needs, was one of the most dramatically elevated genes (Fig.5 d-e). Such upregulation was expected Due to the energy depletion produced by CI malfunction. However, *Pgc1a* was not found in the 17w heart and was unexpectedly downregulated, although the energetic stress was persistent and the necessity of metabolic regulation.

I asked if other cardiac cells responded to *Pgc1a* activation in the same way that cardiomyocytes do. Indeed, a rise in 8w was observed in all cell types, with cardiomyocytes showing the greatest increase. In those cell types, restoration to baseline levels in 17w was also observed (Fig.5 d). However, *Pgc1a* baseline levels in cardiomyocytes were very high in normal conditions compared to no significant expression in other cells, indicating that they have high metabolic requirements and are more susceptible to metabolic insults. Interestingly, visualizing late stress markers and upregulated genes in the 17w genes list such as *Nppb* and *Ankrd1* using UMAP plots, revealed their expression in a small sub-cluster in 8w cardiomyocytes (Fig.5 f). UMAP plots illustrated a shared expression profile between this small sub-cluster of 8w and the 17w cardiomyocytes (Fig.5 g). More surprisingly, the expression of *Pgc1a* was also suppressed (Fig.5 h). I then created a multi-gene UMAP plot of *Pgc1a* and *Ankrd1* (Fig.5 i) showing this suppression to be gradual along the several sub-

clusters on 8w cardiomyocytes, suggesting there might be underlying processes regulating the transitioning to a more maladaptive state like that of 17w.

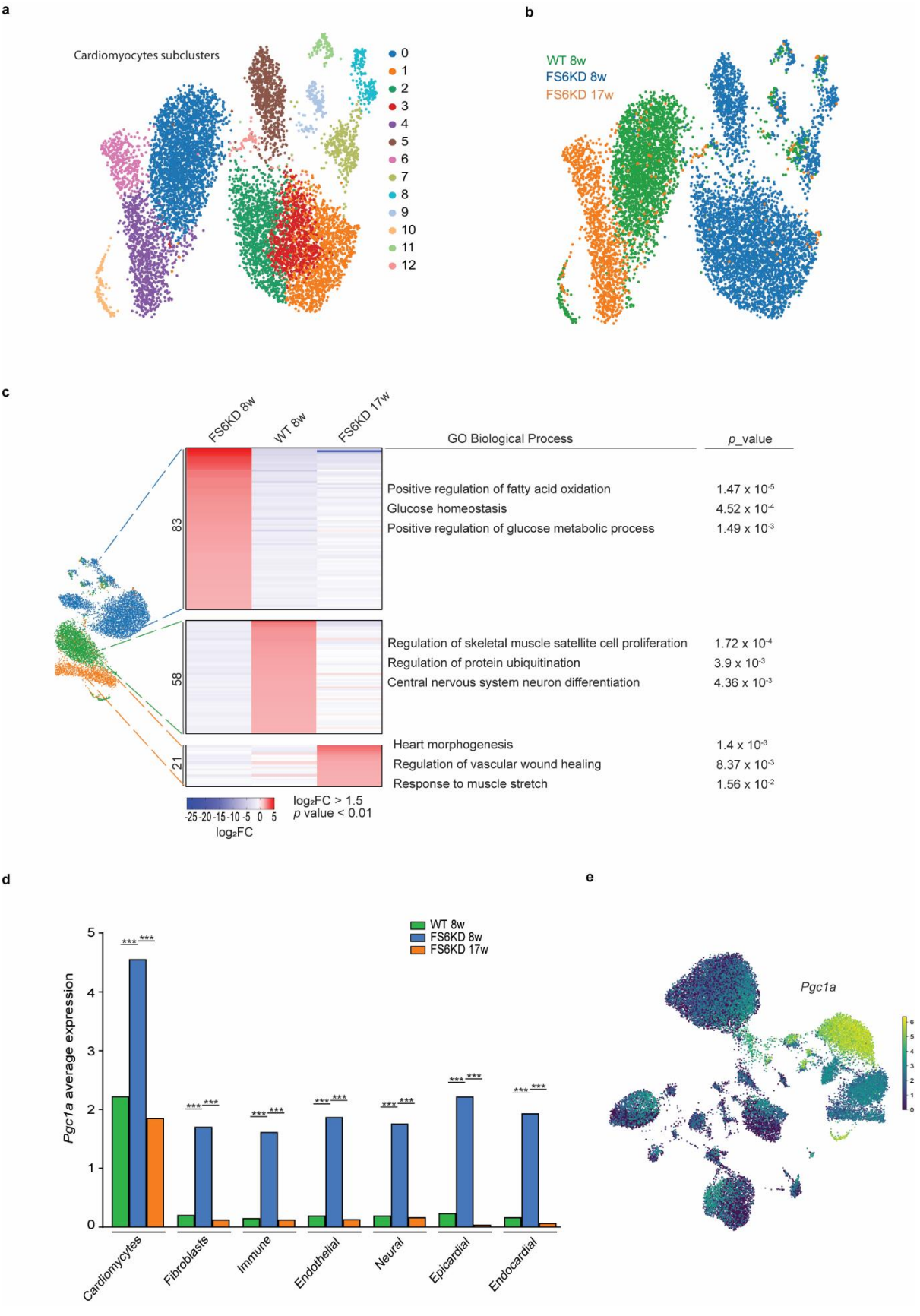

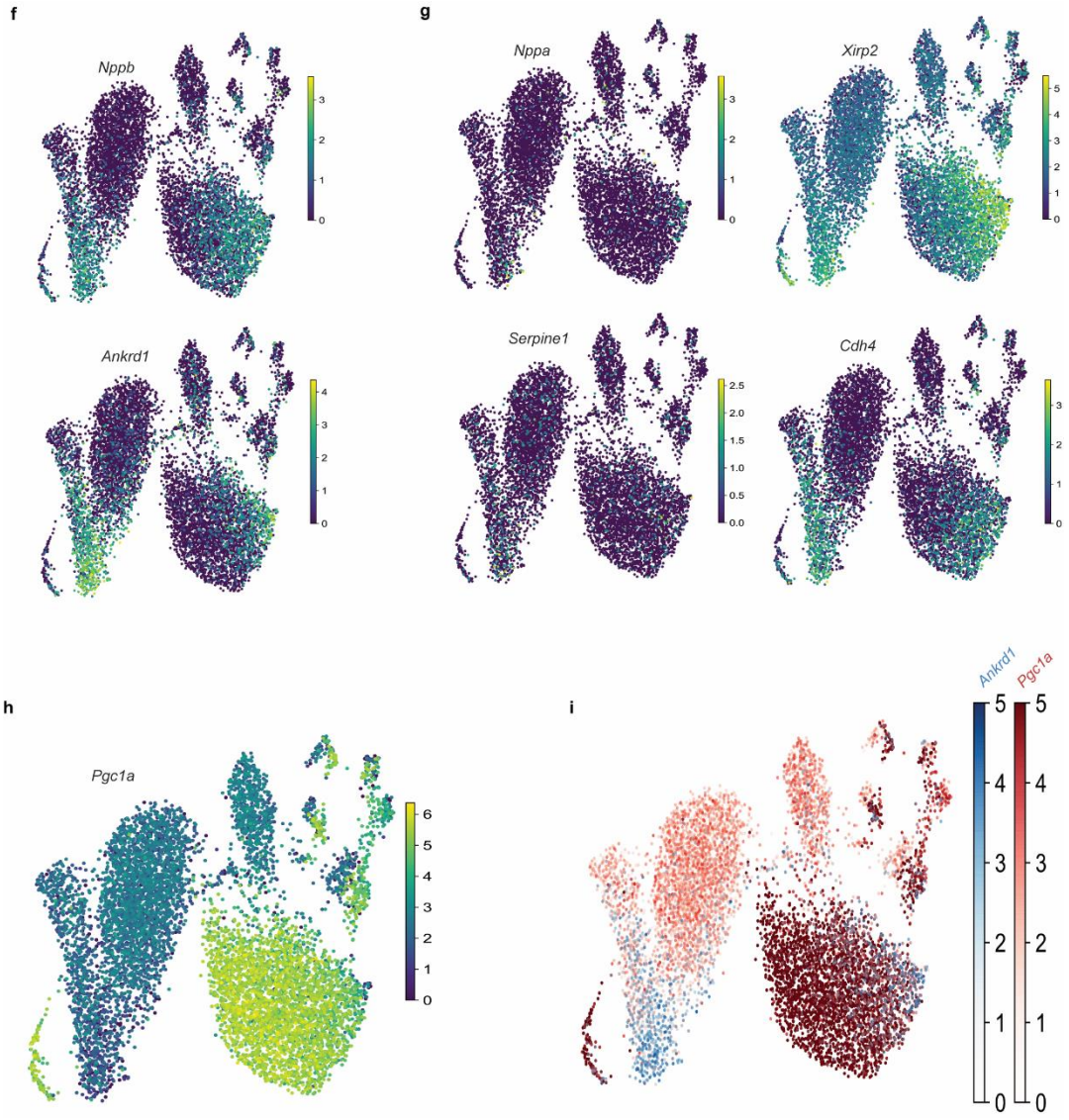


**Fig 5 Identification of a transitioning population in FS6KD 8w**

ComBat integrated datasets UMAP of (a) cardiomyocytes colored by leiden subclusters, and (b) colored by dataset. (c) Heatmap of top expressed DEGs and their associated enriched GO biological processes. (d) Average expression of *Pgc1a* per dataset in total integrated object. UMAP expression gradients of (e) *Pgc1a* in total integrated object, (f) two genes expressed in FS6KD 17w cardiomyocytes of total integrated object, (g) shared genes between FS6KD 17w and small FS6KD 8w subcluster cardiomyocytes of total integrated object, and (h) *Pgc1a* in cardiomyocytes of total integrated object. (i) Multi-gene UMAP expression gradient of *Ankrd1* and *Pgc1a* in cardiomyocytes of total integrated object. Significance is indicated; two-way ANOVA followed by Tukey's post-hoc test. ***$p < 0.001$.

## Trajectory of young FS6KD cardiomyocytes captures dynamic transitioning and cell fate regulation

To confirm if 8w cardiomyocytes are in a transitioning state, I performed pseudo-time trajectory inference analysis using PAGA. Our analysis revealed many cellular states corresponding to different datasets; however, 8w cardiomycoytes contained majority of these states (Fig.6 a). More intriguingly, trajectory analysis revealed a distinct path within the 8w cardiomyocytes comprised of 8 consecutive cell states ordered along a trajectory (Fig.6 b). This path started with cell state number 8 and was followed by states number 5, 6, 4, 7, 12, 10, ending with state number 22. Tracing *Pgc1a* expression along this trajectory revealed a gradual decrease ultimately resulting in downregulation in state 22 (Fig.6 b).

A heatmap of top significantly upregulated genes in the 8w trajectory's cellular states, extracted by DGE analysis, illustrated three phases of expression profiles (Fig.6 c): An early phase, a mid-trajectory phase, and a late more dysfunctional phase. Crucially, I saw dynamic alteration in gene expression patterns where genes expressed in early phase were gradually downregulated and suppressed when mid-states phase genes are expressed. Mid-states genes expression was brief and transient, eventually shutting down and switching gene expression profile to late phase. Late phase states, number 10 and 22, expression profile resembled that of 17w (Fig.5 c), suggesting early states correspond to an adaptive state and this trajectory underlies processes of gene expression regulation leading to a more dysfunctional phenotype.

I further performed GO analysis on DEG of the different trajectory phases (Fig.6 c). Early phase showed enrichment in metabolic processes, regulation of energy homeostasis and fatty acid regulation, while mid-states were enriched in processes regulating the switch to glycolysis, response to oxidative stress and response to wounding, most likely due to cell death. Late phase was enriched in processes responding to lower cardiac output, such as processes involved in muscle stretching and response to DNA damage stress. Early phase and late phase enriched processes corresponded to those of 8w and 17w respectively, further supporting the hypothesis that 8w cardiomyocytes are shifting to dysfunction, and suggesting genes expressed mid-trajectory are the main factors contributing to cellular fate transitioning. Given that driving cell fate is mainly regulated by transcription factors (TFs) or co-factors, I summarized all TFs in the trajectory illustrated in a heatmap (Fig.6 d). From the heatmap, the only TF upregulated mid-states, particularly starting in state 4, and followed by immediate downregulation of *Pgc1a*, was *Atf3*. Other genes expressed mid-trajectory were enzymes or transmembrane channels. Expression visualized by UMAP plot showed a 8w cardiomyocytes-specific expression, zero basal expression, and a complete shutdown at 17w (Fig.6 e). *Atf3* is described as an early stress response factor in the literature[128] and has been demonstrated to have dual transcriptional activity, operating both as an activator and a repressor dependent on co-factors or interacting partners, but primarily as a repressor[128]. Along with our data, this supported the premise of Atf3 as a possible transcription repressor of *Pgc1a* and a main cell fate driver in transitioning to heart failure following metabolic injury.

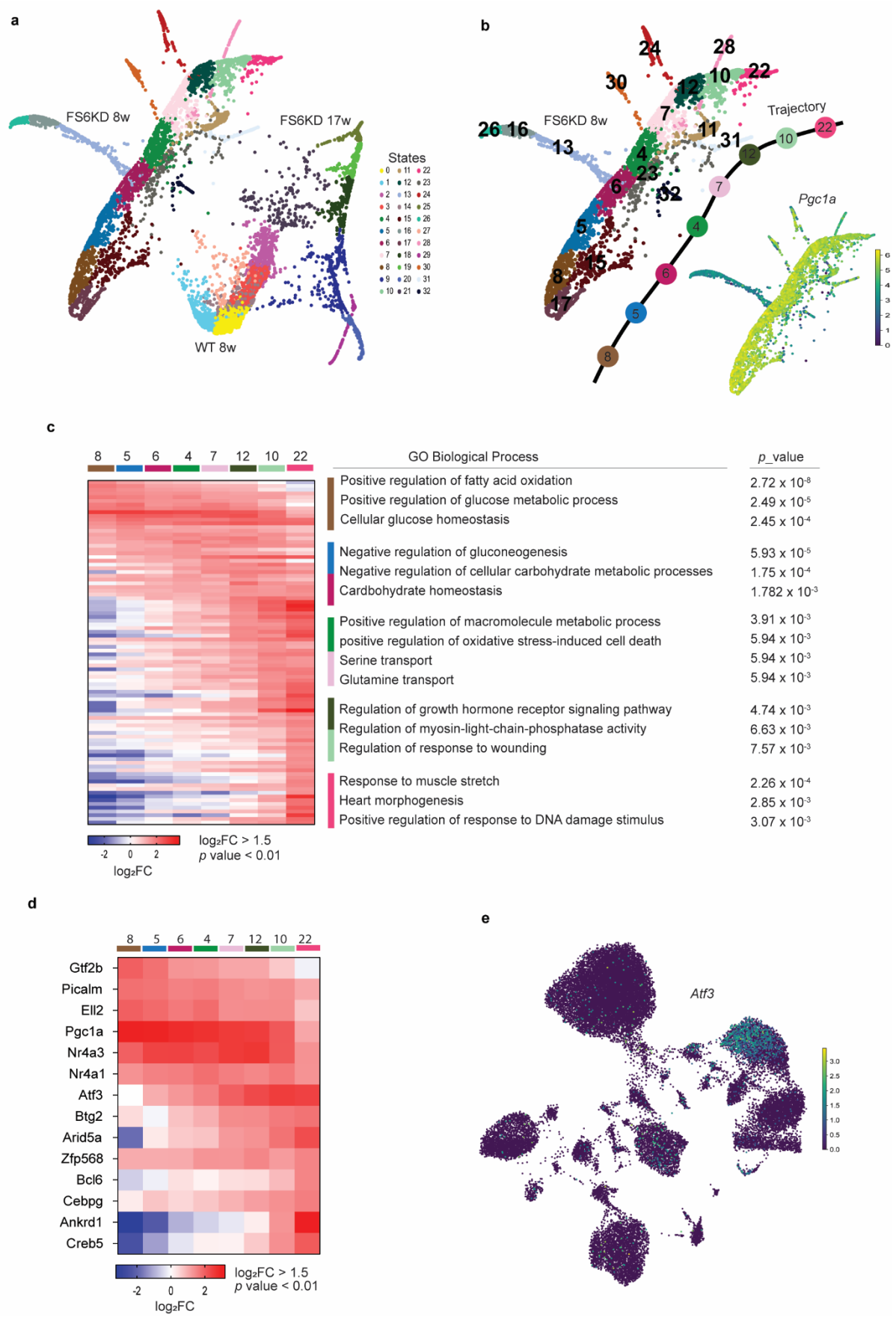


**Fig 6 Identification of Atf3 as a fate decision factor**

FA2 pseudotime trajectory graph calculated by PAGA for (a) cardiomyocytes of three ComBat integrated datasets colored by cell states, and (b) isolated FS6KD 8w with expression gradient of *Pgc1a*. (c) Heatmap of top expressed DEGs in trajectory states of FS6KD 8w and their associated enriched GO biological processes. (d) Heatmap of transcription factors and cofactors extracted from trajectory's DEGs. (e) UMAP expression gradient of *Atf3* in total integrated object.

## Atf3 supresses Pgc1a and governs tissue to malfunction

To corroborate *Atf3* spatiotemporal expression in cardiac tissue, I experimentally validated our trajectory results by performing series of heart immunostaining experiments. First, I stained tissue sections from 8w FS6KD with anti-cardiac troponin I type 3 antibody (TnnI3), a marker gene exclusively expressed in cardiomyocytes, to confirm Atf3 cellular localization. Nuclei expressing Signal of Atf3 was only observed in nuclei of cells expressing TnnI3, confirming its cardiomyocytes localization (Fig.7 a).

To visualize basal Atf3 protein levels and expression pattern, I stained tissues from WT, FS6KD 6w and older 10w hearts. I detected Atf3 signal in form of nuclei clusters spread across 6w heart tissue (Fig.7 b) but not in WT or 10w, suggesting Atf3 was expressed in response to metabolic stress. I also observed differences in signal intensity in Atf3-positive cells within individual clusters; signal was strongest in the center and weakened gradually in nuclei located periphery of the cluster. This pattern of expression was seen in all aggregates, suggesting Atf3 expression indeed is gradual similar to what was seen in the trajectory.

Furthermore, I stained with anti-Pgc1a antibody to assess Pgc1a expression in these tissues, especially in Atf3-positive clusters. I observed Pgc1a expression to be higher in regions outside of the clusters where there is no Atf3 expression (Fig.7 c). Inside the aggregates, I found a smaller number of Pgc1a-positive nuclei that also showed weaker level of expression compared to Pgc1a-positive nuclei in Atf3-negative regions. To better visualize this contrast in expression level, I counted Atf3-positive, Pgc1a-positive, and double-stained nuclei in three different FS6KD tissues. About 80% of all nuclei were found to either express Atf3 or pgc1a exclusively, however, less than half showed co-localization of expression (Fig.7 d). These data confirmed tissue expression resembled expression levels in different states along our trajectory, starting from high Pgc1a expression early phase, an intermediate state of Atf3 expression where Pgc1a expression is still high, and a late phase where cellular states have suppressed level of Pgc1a but high Atf3 expression.

Simultaneously, I performed spatial transcriptomics using photo-isolation chemistry[123] (PIC) to investigate contrasting *Atf3* expression levels within Atf3-positive aggregates. In addition to identifying gene expression profiles, I aimed to minimize any potential biases generated by IHC signal measurement or differences in protein stability. Individual cells within the Atf3-positive clusters were chosen for additional library preparation and sequencing based on their Atf3 signal intensity; Atf3-high cells and Atf3-low cells. I first confirmed that *Atf3* expression levels were higher in datasets selected for high Atf3 signal (Fig.7 e). Then I looked at *Pgc1a* expression, as well as genes expressed late in our trajectory such *Nppb* and *Ankrd1*.

*Pgc1a* levels were higher in Atf3-low regions and indeed lower in Atf3-high regions. *Nppb* and *Ankrd1* levels, on the other hand, increased in Atf3-high cells. Furthermore, GO analysis revealed that Atf3-high expressing cells had higher metabolic dysfunction, lower oxidative phosphorylation, and lower cardiac contractility (Fig.7 f). Despite being in proximity, the profiles of contrasting cells reflected processes that were enhanced in early versus late trajectory states and in 8w versus 17w.

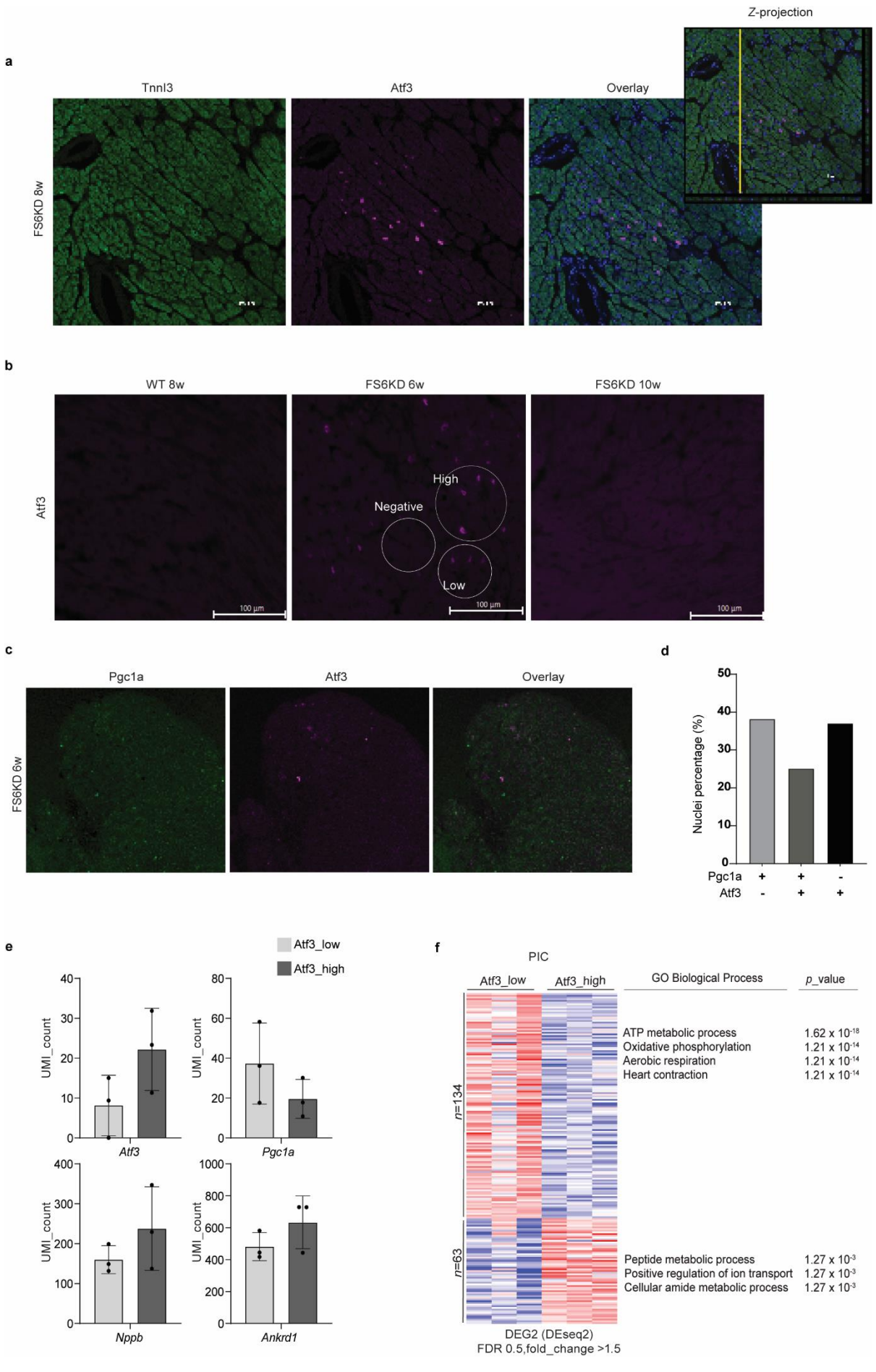
a
Z-projection
TnnI3
Atf3
Overlay
FS6KD 8w
b
WT 8w
FS6KD 6w
FS6KD 10w
Atf3
High
Negative
Low
100 μm
c
Pgc1a
Atf3
Overlay
FS6KD 6w
d
Nuclei percentage (%)
50
40
30
20
10
0
Pgc1a + + -
Atf3 - + +
e
Atf3_low
Atf3_high
UMI_count
Atf3
Pgc1a
Nppb
Ankrd1
f
PIC
Atf3_low
Atf3_high
GO Biological Process
p_value
ATP metabolic process 1.62 x 10-18
Oxidative phosphorylation 1.21 x 10-14
Aerobic respiration 1.21 x 10-14
Heart contraction 1.21 x 10-14
n=134
n=63
Peptide metabolic process 1.27 x 10-3
Positive regulation of ion transport 1.27 x 10-3
Cellular amide metabolic process 1.27 x 10-3
DEG2 (DEseq2)
FDR 0.5,fold_change >1.5

**Fig 7 Validating Atf3 in-vivo**

Immunostained images of female heart tissue with (a) TnnI3 antibody and Atf3 antibody, with peripheral nuclei Z-projection of 8 1um layers, Representative images from seven tissues were shown (x20 magnification). (b) Atf3 antibody. Representative images from three individuals and five tissues were shown (x20 magnification), and (c) Pgc1a antibody and Atf3 antibody. Representative images from over 20 sections were shown (x20 magnification). (d) Percentage of nuclei expressing either Pgc1a, Atf3 or both counted from 28 sections. PIC identified (e) UMI counts of different targets in low vs high Atf3 expression groups (n = 3), and a (f) Heatmap of top expressed DEGs and their associated enriched GO biological processes.

## Atf3 is the principal response factor in CI deficiency mitochondrial cardiomyopathy

Atf3 belongs to the ATF/CREB transcription factor family[128], which members have been demonstrated to be central stress response factors in a variety of disease models, including metabolic disorders[99,102]. Only *Atf3* was shown to be significantly increased in our DEG lists, but I saw upregulation of other *ATF* genes in FS6KD populations, including *Atf4*, *Atf5*, and *Atf6* on UMAP plots (Fig.8 a). None of these genes displayed the cellular specificity found with *Atf3* cardiomyocytes expression, however I did find enhanced expression of both *Atf4* and *Atf5* in fibroblasts. I measured mRNA levels of *Atf3*, *Atf4*, *Atf5*, and *Atf6* in whole cardiac tissues of WT, 6w to 18w female, and 6w to 29w male FS6KD mice to compare their span of expression and levels along disease progression. Similar to findings from snRNA-seq data and tissue staining, *Atf3* had extremely low basal expression and FS6KD induction was early and transient in both female and male mice, emphasizing its responsive nature and role as a driver of cellular fate determination (Fig.8 b, f). Only the expression pattern of *Atf4* resembled that of *Atf3* in tissues obtained from female mice. I observed that WT mice had low *Atf4* basal expression, which was followed by an early increase in 6-8w mice, then repressed back to basal levels in older mice (Fig.7 c). *Atf5* response was slower and sustained for a longer period of time. Although I observed a significant upregulation starting 9w, it was not as dramatic as *Atf3* or *Atf4* (Fig.7 d). Finally, *Atf6* expression was inhibited starting 13w rather than induced (Fig.8 e). Basal WT expression levels was varied between the 4 genes and was the highest in *Atf6*. Expression patterns of *Atf4*, *Atf5* and *Atf6* in male FS6KD mice were consistent (Fig.8 g-i); I observed late expression surge starting 9w that was not suppressed and was maintained up to 29w. Male mice had a substantially lower basal level in all evaluated *ATF* members when compared to female mice.

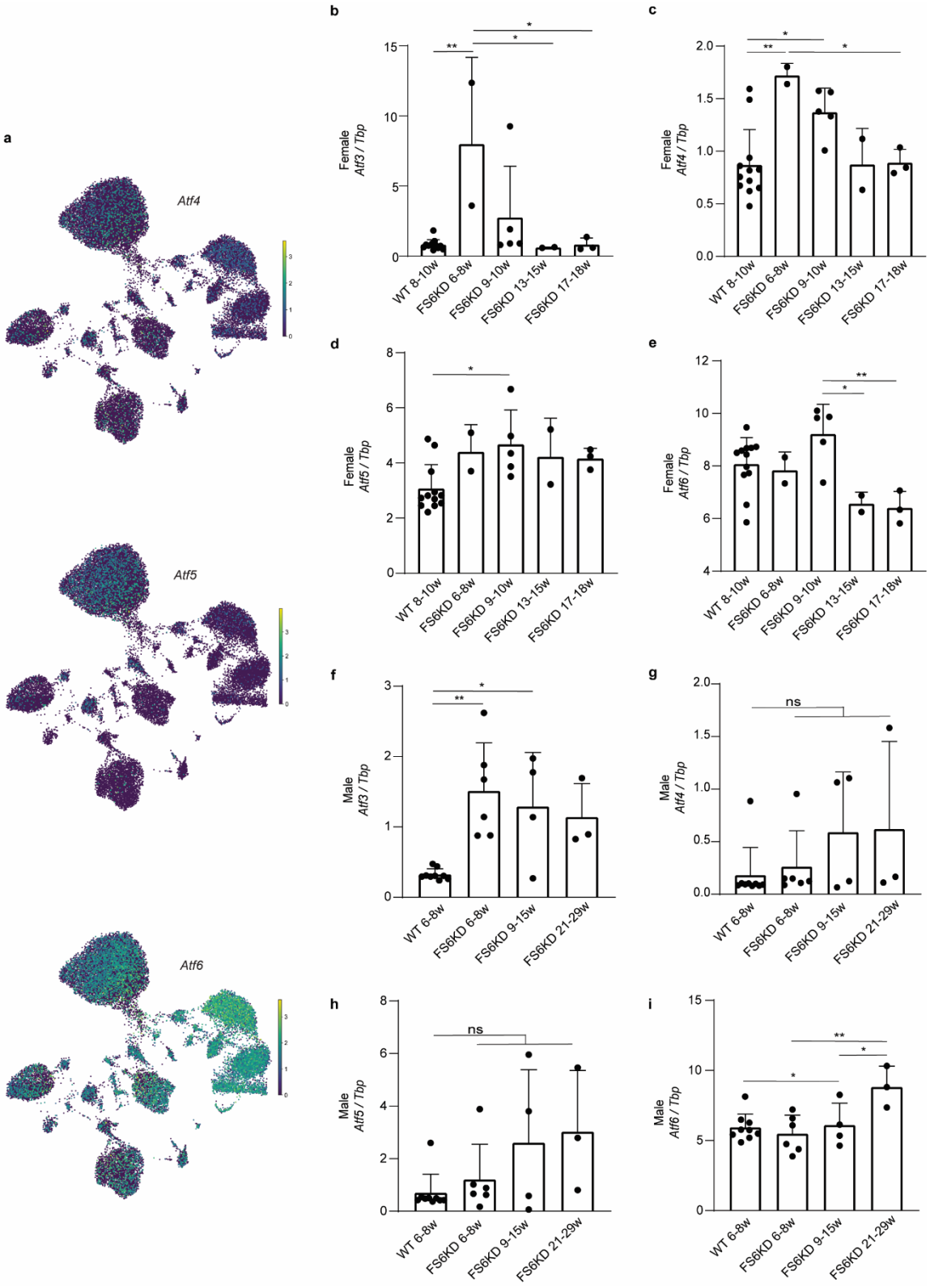
a
Atf4
Atf5
Atf6
b
Female
Atf3 / Tbp
WT 8-10w
FS6KD 6-8w
FS6KD 9-10w
FS6KD 13-15w
FS6KD 17-18w
c
Female
Atf4 / Tbp
d
Female
Atf5 / Tbp
e
Female
Atf6 / Tbp
f
Male
Atf3 / Tbp
WT 6-8w
FS6KD 6-8w
FS6KD 9-15w
FS6KD 21-29w
g
Male
Atf4 / Tbp
ns
h
Male
Atf5 / Tbp
i
Male
Atf6 / Tbp

**Fig 8 Evaluation of other ISR$^{mt}$ genes**

(a) UMAP expression gradients of *Atf4, Atf5*, and *Atf6* in total integrated object. Female heart tissue of different time points for (b) *Atf3,* (c) *Atf4,* (d) *Atf5*, and (e) *Atf6* expression analyzed by ddPCR and normalized to *Tbp* expression ($n \geq 3$ per group, FS6KD 6-8w and 13-15w $n = 2$). Male heart tissue of different time points for (f) *Atf3*, (g) *Atf4,* (h) *Atf5*, and (i) *Atf6* expression analyzed by ddPCR and normalized to *Tbp* expression ($n \geq 3$ per group). Significance is indicated; one-way ANOVA followed by Tukey's post-hoc test. $*p < 0.05$, $**p < 0.01$, ns: not significant.

*Atf3* expression was established to be the earliest of the *ATF* genes in snRNA-seq analysis, while the other members are expressed secondary to *Atf3*. Expression levels seen from bulk mRNA also showed their levels to be downregulated in the 17w FS6KD hearts. Thus, I introduced and integrated a 12w FS6KD with FS6KD datasets to observe the upregulation course over three time points. Shifting of 12w cardiomyocytes cluster positioned intermediate of 8w and 17w was visualized by UMAP plot (Fig.9 a), further confirming 8w transitioning has already been completed. *Atf3* was supressed in 12w, while *Atf4, Atf5*, and *Atf6* expression levels peaked at 12w and were downregulated in 17w (Fig.9 b,d). *Atf4* is one of the effectors of the ISR$^{mt}$ and can in turn induce expression of other downstream effectors. None of these genes were expressed early (Fig.9 c,d) and their expression also peaked at 12w, including *Gdf15* and *Fgf21*, strongly supporting *Atf3* as the early and primary modulator of stress response not the ISR$^{mt}$ program.

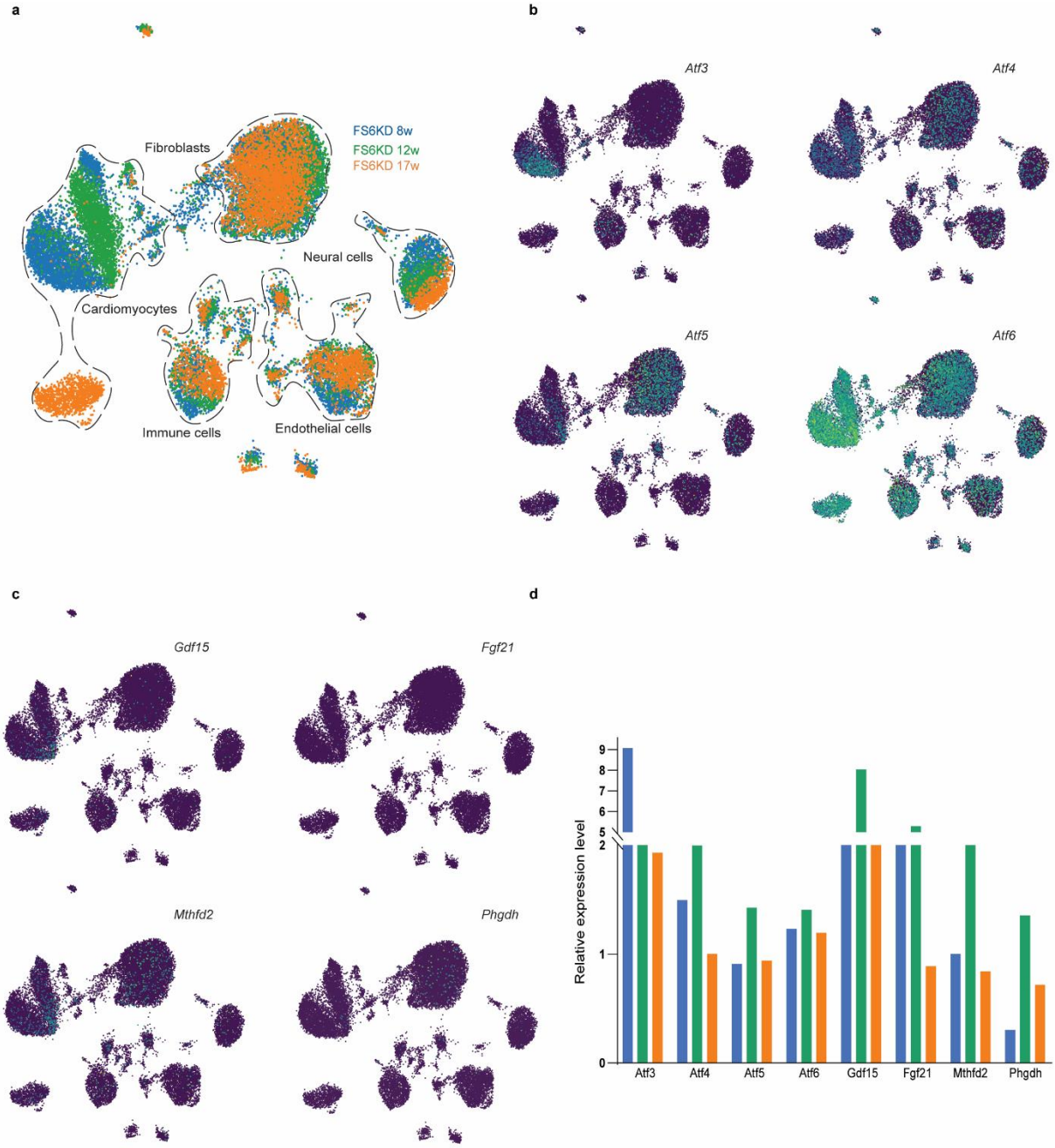


**Fig 9 ISRmt is downstream of Atf3 activation**

(a) ComBat integrated datasets UMAP of 8w, 12w, and 17w FS6KD cardiac cellular populations colored by dataset. UMAP expression gradients of (b) *Atf3*, *Atf4*, *Atf5*, and *Atf6*, and (c) *Gdf15*, *Fgf21*, *Mthfd2* and *Phgdh* in total integrated object. (d) Relative expression levels normalized to WT expression.

## Metabolic stress is the only factor inducing shifting in cellular states of FS6KD.

The data obtained so far suggest that cardiomyocytes shifting was a result of dynamic changes in transcriptional profiles modulated by the transcriptional regulator Atf3 in response to metabolic stress. To further confirm it and exclude the possibility that gene expression changes were not influenced by age, I integrated two WT datasets of 8w and 17w. Unsupervised clustering showed a complete cluster fitting with no shifting in any cellular population (Fig.10 a), particularly in cardiomyocytes. Additionally, gene expression levels of genes found upregulated in the FS6KD 8w or 17w DEG lists were not changed in either of the WT datasets (Fig.10 c). To further confirm lack of any algorithm bias during integration caused by presence of WT dataset, I integrated only 8w and 17w FS6KD datasets. Shifting was observed on UMAP plots after clustering similar to the 3-dataset integrated object (Fig.10 b). These data suggested the observed shifting in cellular states accompanied by changing gene expression was not induced by age nor due to bias in integration.

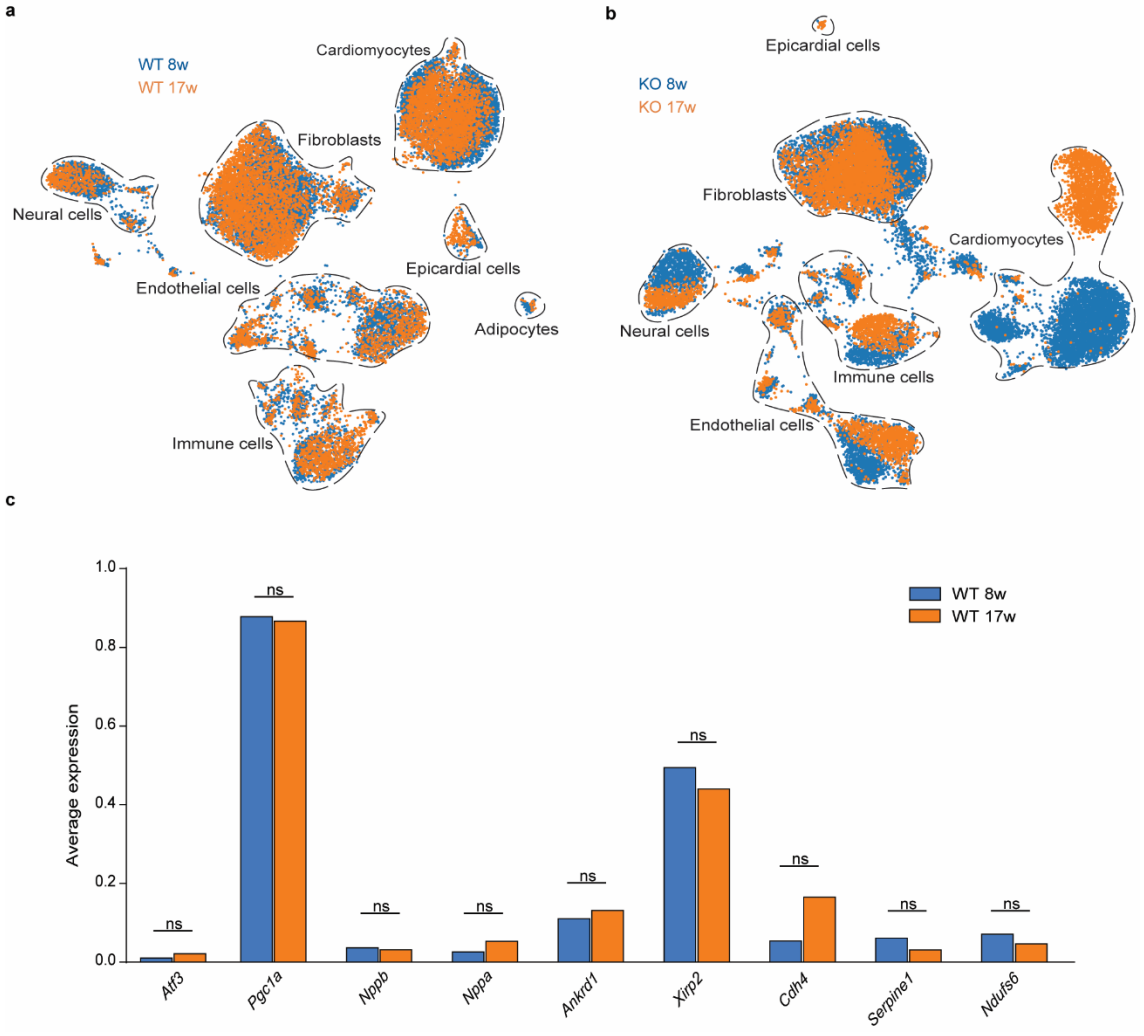


**Fig 10 Cellular landscape of young vs old healthy mice**

ComBat integrated datasets UMAP of (a) 8w and 17w WT cardiac cellular populations colored by dataset, and (b) 8w and 17w FS6KD cardiac cellular populations colored by dataset. (c) Average expression per WT dataset in total integrated object of genes extracted from 8w or 17w FS6KD DEG lists.

# Loss of *Atf3* enhances cardiac function and elevates ejection fraction

To assess if lack of Atf3 under OXPHOS dysfunction halts transitioning, and thus phenotype progression, to a more dysfunctional state, we introduced large deletion from exon 1 to exon 3 of *Atf3* gene by CRISPR/Cas9 in FS6KD fertilized eggs and evaluated cardiac phenotype starting 8 weeks of age. As expected, complete loss of *Atf3* preserved ejection fraction and enhanced cardiac function (Fig11. a-c) compared to the heterozygous Atf3 littermates, suggesting that the presence of Atf3 is sufficient to induce transitioning into dysfunction.

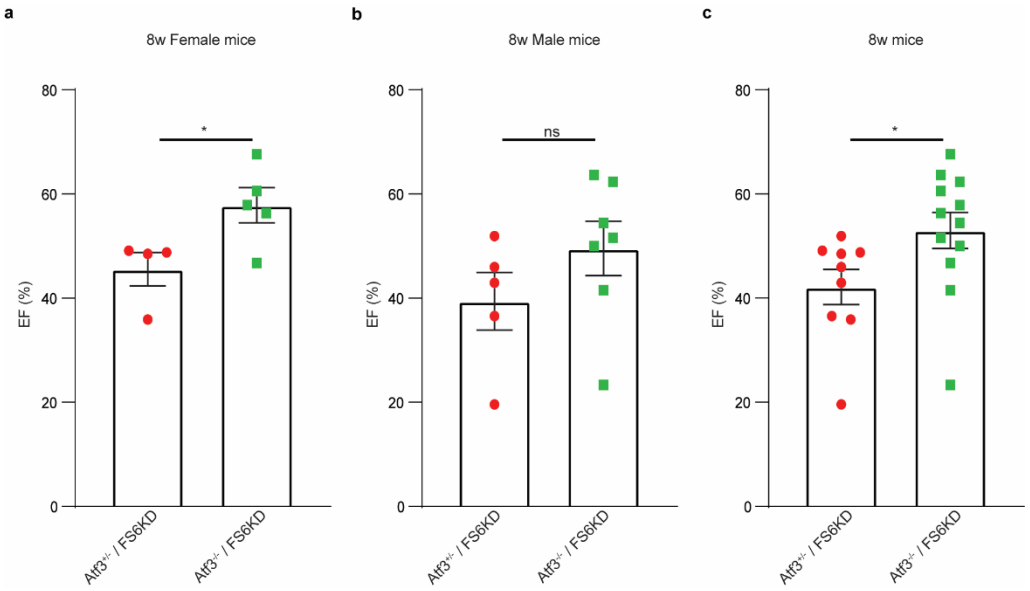


**Figure 11 Atf3 promotes cardiac dysfunction**

(a) Left ventricular ejection fraction of Atf3 knockout/FS6KD (a) female mice ($n \geq 3$), (b) male mice ($n \geq 3$), and (c) all mice ($n \geq 3$). Significance is indicated; t-test. $*p < 0.05$, ns : not significant.

# Discussion

Identifying factors that contribute to the termination of early endogenous regulatory machines in response to mitochondrial malfunction, necessitates late onset disease models that may be employed for early to late tracing. We performed single cell transcriptomics on the hearts of *Ndufs6*$^{gt/gt}$ cardiac-specific CI deficiency mice with differing cardiac function, then used the ScanPY analytical platform to perform integration, clustering, DEG analysis, and pseudotime trajectory analysis. The results show that CI-dysfunction in the heart promotes *Pgc1a* upregulation to regulate mitochondrial biogenesis and modulates glucose metabolism to establish metabolic homeostasis. *Pgc1a* suppression has been found to be a crucial point in tissue malfunction. The trajectory of FS6KD 8w cardiomyocytes demonstrated dynamic transcriptional reprogramming that was controlled by transient expression of the Atf3 transcription factor. This strongly supports the hypothesis that Atf3 serves as a transcriptional suppressor of *Pgc1a* in cardiomyocytes as a primary stress response.

To our knowledge, there are no previous reports on the direct role of Atf3 in MDs or as a modulator of *Pgc1a*. Role of Atf3 as an early stress response modulator was reported in many disease models of heart failure[129–131], cardiomyopathies[132–134], and ischemia/reperfusion injuries[135–137], with an ongoing debate on whether this role is beneficial or detrimental for tissue remodelling and pathogenesis. In addition, its controversial induction outcomes are observed in many other diseases like cancers and inflammation[138], and tissues like kidney[139,140] and liver[141,142]. Some studies showed Atf3 to have a function in regulating glucose metabolism. For example, Atf3 expression was protective in cardiomyocytes of high fat diet treated mice by control of glucose tolerance and decreasing insulin resistance[143]. However, role of Atf3 is rarely observed in the context of MD. Aside from one recent report showing a slight increase in much later stages of a multi-cascade ISR$^{mt}$ response[99] in Deletor mouse. The reported timing of expression contradicted the overwhelming body of evidence indicating Atf3 as an early responder after insult or injury; this could be due to a secondary involvement as an interacting partner for another TF. ISR$^{mt}$ genes are the more commonly seen as the earliest responders in MDs, especially in severe metabolic defects. This could be because 1) most models exhibit an early onset and rapidly progressive disease phenotype, or 2) tissues are examined after severe phenotypes are evident, implying that tissues have already transitioned.

In accordance with the hypothesis, metabolic dysfunction prompted different responses in different cardiac cellular populations, resulting in variable outcomes to CI deficiency. Cardiomyocytes had the greatest change in gene expression profiles of the three datasets, as seen by the significant shift in landscape. Although *Pgc1a* induction was identified in all cell types as an endogenous mechanism for maintaining metabolic homeostasis, Atf3 upregulation was only observed in cardiomyocytes. One reason could be because cardiomyocytes are more metabolically demanding, thus more susceptible to perturbations in energy homeostasis. Basal *Pgc1a* expression was indeed found to be higher in cardiomyocytes, indicating that mitochondrial regulation is active and persistent. Furthermore, the metabolic shifting induced by Pgc1a might have been sufficient to restore balance in other cells. Nonetheless, the possibility of different cell types triggering different responses regardless of their metabolic demands cannot be excluded. There are many targets downstream of Atf3[134], in addition to its

potential to form a heterodimer with other TFs[144], Atf3 activation in cardiomyocytes could have had secondary effects that contributed to the adverse phenotype.

Many studies investigated the effect of *Pgc1a* overexpression on mitochondrial content, function, and regulation of metabolism, as a therapeutic approach. While some studies demonstrated increase in mitochondrial content[145], improving glucose tolerance and muscle weakness[146], others reported no effect on either glucose intolerance or induced obesity[147]. Most importantly, these observations were for short term effects and their effects on the long run were not considered. In addition, *Pgc1a* overexpression in the liver caused insulin resistance, highlighting detrimental side effects of *Pgc1a* systemic overexpression[148]. In MD models, pharmacological induction of *Pgc1a* using bezafibrate yielded either very weak positive effects or no beneficial response, accompanied by adverse side effects due to bezafibrate toxicity on the liver[149,150]. In the heart, overexpression of *Pgc1a* in a cardiac specific manner led to detrimental effects such as cardiomyopathy[151,152] when established in adult mice. However, heart specific overexpression while in the neonatal stage enhanced mitochondrial proliferation. These age-dependent outcomes suggest presence of a functional working window that should be further considered. On the other hand, fine-tuning Pgc1a dosage with modest cardiomyocyte specific expression was shown to promote mitochondrial function in a telomerase-deficient aging mouse model, in addition to elevating cardiac function and significantly extending health span[153]. Literature thus highlights the unfeasibility of *Pgc1a* overexpression as a therapeutic target, but the targeting of cell specific regulators that allows for continuous endogenous levels of expression being more ideal.

Despite the fact that *Pgc1a* induction was highest in cardiomyocytes, the surge and suppression trend was observed in other cells. This can be explained by the expression of other ATF family members involved in $ISR^{mt}$ and $UPR^{mt}$, namely *Atf4*, *Atf5*, and *Atf6*. Although their expression was not significant and had no cellular specificity, increased levels in specific cells were seen, such as *Atf5* in fibroblasts. Their basal expression was also very high in comparison to the extremely low levels of *Atf3*, and their upregulation occurred later and more steadily, implying that they do not function as the primary stress response mechanism, but rather that their activation serves as a long-term adaptive response. The transient expression of *Atf3* might also be a predecessor of $ISR^{mt}$ activation acting as a triggering factor, and because of their fast progression phenotypes and experimental design, previous MD models may have easily overlooked its expression.

Finally, FS6KD model did not show significant FGF21 expression. Although FGF21 induction is common in mitochondrial myopathies caused by mtDNA defects, it is generally lower and less common in mice or humans with ETC structural abnormalities[154]. Moreover, a recent comprehensive investigation[104] on several mitochondrial dysfunction models demonstrated that FGF21 modulates stress responses in mild or moderate OXPHOS failure, but is not required for stress response in severe models.

## Significance

Recent consensus strongly demonstrates response to mitochondrial dysfunctions varies between different tissue types[97,99,104]. This work highlights an even higher layer of specificity to mitochondrial stress response, where individual cells resident of one tissue can elicit distinct reactions to same stressor and illustrates differences in cellular dependency on mitochondrial respiration. Furthermore, it recognizes molecular players in very early stages of disease that can be targeted for future therapeutic endeavours.

## Limitations and future directions

FS6KD mouse model allowed tracing the cardiac manifestation of CI deficiency-induced MDs and helped in identifying earlier responses than previously suggested. However, since this model is cardiac specific, the effect of CI deficiency cannot be observed in other metabolically demanding tissues like the brain. As a result, it is impossible to predict if these disparities in responses are generalizable or whether Atf3 is also involved in the progression of the disease in other tissues. It is also unknown whether *Pgc1a* upregulation is utilized by other tissues for metabolic regulation under stress.

This study is a pioneer in using single cell transcriptomics to characterize mitochondrial cardiomyopathies. The effective identification of cellular modulators opens numerous possibilities for future research. One is the investigation of CI deficiency in other tissues, as well as the intricacy of multi-tissue responses in systemic disease models. Furthermore, future research could focus on comprehensively identifying responses to different ETC complexes induced by OXPHOS dysfunction.

## Conclusions

This study shows that *Atf3* expression in cardiomyocytes following CI dysfunction in the heart has a detrimental impact and plays a role in disease development by suppressing *Pgc1a* upregulation, a cellular adaptive regulatory mechanism. Although early endogenous adaptive mechanisms were shared among cardiac cellular populations, stress response pathways were distinct, suggesting presence of different factors committing cells to dysfunction prior to the activation of the conventional long-term $ISR^{mt}$ cascade. In conclusion, these findings support the importance of cellular resolutions in understanding heterogeneous disorders such as MDs, and in identifying targets for therapy.

# References


1. Gabaldo, T. Proto-Mitochondrial Metabolism. **301**, (2003).
2. Chinnery, P. F. & Lightowlers, R. N. Reanalysis and revision of the Cambridge reference sequence for human mitochondrial DNA. **23**, 3965 (1999).
3. Hensen, F., Cansiz, S., Gerhold, J. M. & Spelbrink, J. N. Biochimie To be or not to be a nucleoid protein : A comparison of mass- spectrometry based approaches in the identi fi cation of potential mtDNA-nucleoid associated proteins. *Biochimie* **100**, 219–226 (2014).
4. Morgenstern, M. *et al.* Definition of a High-Confidence Mitochondrial Proteome at Quantitative Scale Resource Definition of a High-Confidence Mitochondrial Proteome at Quantitative Scale. 2836–2852 (2017) doi:10.1016/j.celrep.2017.06.014.
5. Kasamatsu, H. & Vinograd, J. REPLICATION OF CIRCULAR 1DNA IN EUKARYOTIC CELLS. (1974) doi:10.1146/annurev.bi.43.070174.003403.
6. Neupert, W. & Herrmann, J. M. Translocation of Proteins into Mitochondria. (2007) doi:10.1146/annurev.biochem.76.052705.163409.
7. Taanman, J., Street, R. H. & Nw, L. The mitochondrial genome : structure , transcription , translation and replication. **1410**, (1999).
8. Osellame, L. D., Blacker, T. S. & Duchen, M. R. Cellular and molecular mechanisms of mitochondrial function. *Best Pract. Res. Clin. Endocrinol. Metab.* **26**, 711–723 (2012).
9. Hatefi, Y. THE MITOCHONDRIAL ELECTRON TRANSPORT AND OXIDATIVE PHOSPHORYLATION SYSTEM. (1985) doi:https://doi.org/10.1146/annurev.bi.54.070185.005055.
10. Chinnery, P. F. & Hudson, G. Mitochondrial genetics. 135–159 (2013) doi:10.1093/bmb/ldt017.
11. Brien, T. W. O. Evolution of a protein-rich mitochondrial ribosome : implications for human genetic disease. **286**, 73–79 (2002).
12. Tang, J. X., Thompson, K. & Taylor, R. W. Mitochondrial OXPHOS Biogenesis : Co-Regulation of Protein Synthesis , Import , and Assembly Pathways. (2020).
13. Herst, P. M., Rowe, M. R., Carson, G. M. & Berridge, M. V. Functional mitochondria in health and disease. *Front. Endocrinol. (Lausanne).* **8**, (2017).
14. Mayr, J. A. *et al.* Spectrum of combined respiratory chain defects. 629–640 (2015) doi:10.1007/s10545-015-9831-y.
15. Gorman, G. S. *et al.* Mitochondrial diseases. *Nat. Rev. Dis. Prim. 2016 21* **2**, 1–22 (2016).
16. Craven, L., Alston, C. L., Taylor, R. W. & Turnbull, D. M. Recent Advances in Mitochondrial Disease. *Annu. Rev. Genomics Hum. Genet.* **18**, 257–275 (2017).
17. Science, T. G. *et al.* Ubiquitin tag for sperm mitochondria. **2005**, 1998–1999 (2005).

18. Rossignol, R., Malgat, M., Mazat, J. & Letellier, T. Threshold Effect and Tissue Specificity. *J. Biol. Chem.* **274**, 33426–33432 (1999).

19. White, S. L. *et al.* Genetic Counseling and Prenatal Diagnosis for the Mitochondrial DNA Mutations at Nucleotide 8993. 474–482 (1999) doi:https://doi.org/10.1086/302488.

20. Munaro, M. *et al.* A single cell complementation class is common to several cases of cytochrome c oxidase-defective Leigh's syndrome. *Hum. Mol. Genet.* **6**, 221–228 (1997).

21. Tatlisumak, T. *et al.* Frequency of MELAS main mutation in a phenotype-targeted young ischemic stroke patient population. *J. Neurol.* **263**, 257–262 (2016).

22. Anderson, N. S. & Haynes, C. M. Folding the Mitochondrial UPR into the Integrated Stress Response. *Trends Cell Biol.* **30**, 428–439 (2020).

23. Wallace, D. C. *et al.* Mitochondrial DNA Mutation Associated with Leber's Hereditary Optic Neuropathy. **729**, (1987).

24. Shoffner, J. M. *et al.* Myoclonic epilepsy and ragged-red fiber disease (MERRF) is associated with a mitochondrial DNA tRNALys mutation. *Cell* **61**, 931–937 (1990).

25. Holt, I. J., Harding, A. E., Petty, R. K. H. & Morgan-Hughes, J. A. A new mitochondrial disease associated with mitochondrial DNA heteroplasmy. *Am. J. Hum. Genet.* **46**, 428–433 (1990).

26. Zeviani, M. & Di Donato, S. Mitochondrial disorders. *Brain* **127**, 2153–2172 (2004).

27. Mattman, A. *et al.* Mitochondrial disease cilincal mannifestation- an overview. 183–187 (2011).

28. Nesbitt, V. *et al.* The UK MRC Mitochondrial Disease Patient Cohort Study: Clinical phenotypes associated with the m.3243A>G mutation - Implications for diagnosis and management. *J. Neurol. Neurosurg. Psychiatry* **84**, 936–938 (2013).

29. Schlieben, L. D. & Prokisch, H. The Dimensions of Primary Mitochondrial Disorders. *Front. Cell Dev. Biol.* **8**, 1–11 (2020).

30. Rahman, J., Noronha, A., Thiele, I. & Rahman, S. Leigh map: A novel computational diagnostic resource for mitochondrial disease. *Ann. Neurol.* **81**, 9–16 (2017).

31. Robinson, B. H. Lacticacidemia. **1182**, 231–244 (1993).

32. Bourgeron, T. *et al.* Mutation of a nuclear succinate dehydrogenase gene results in mitochondrial respiratory chain deficiency. **11**, (1995).

33. Patrick, K. L. 454 Life Sciences: Illuminating the future of genome sequencing and personalized medicine. *Yale J. Biol. Med.* **80**, 191–194 (2007).

34. Applegarth, D. A., Toone, J. R. & Lowry, R. B. Incidence of Inborn Errors of Metabolism in British Columbia , 1969-1996 Incidence of Inborn Errors of Metabolism in British Columbia , 1969 − 1996 The online version of this article , along with updated information and services , is located on the World . (2014) doi:10.1542/peds.105.1.e10.

35. Darin, N., Oldfors, A., Moslemi, A. R., Holme, E. & Tulinius, M. The incidence of

mitochondrial encephalomyopathies in childhood: Clinical features and morphological, biochemical, and DNA abnormalities. *Ann. Neurol.* **49**, 377–383 (2001).

36. Skladal, D., Halliday, J. & Thorburn, D. R. Minimum birth prevalence of mitochondrial respiratory chain disorders in children. *Brain* **126**, 1905–1912 (2003).

37. Schaefer, A. M. *et al.* Prevalence of mitochondrial DNA disease in adults. *Ann. Neurol.* **63**, 35–39 (2008).

38. Elliott, H. R., Samuels, D. C., Eden, J. A., Relton, C. L. & Chinnery, P. F. Pathogenic Mitochondrial DNA Mutations Are Common in the General Population. *Am. J. Hum. Genet.* **83**, 254–260 (2008).

39. Gorman, G. S. *et al.* Prevalence of nuclear and mitochondrial DNA mutations related to adult mitochondrial disease. *Ann. Neurol.* **77**, 753–759 (2015).

40. Buajitti, E., Rosella, L. C., Zabzuni, E., Trevor Young, L. & Andreazza, A. C. Prevalence and health care costs of mitochondrial disease in Ontario, Canada: A population-based cohort study. *PLoS One* **17**, 1–9 (2022).

41. Yamazaki, T. *et al.* Molecular diagnosis of mitochondrial respiratory chain disorders in Japan: Focusing on mitochondrial DNA depletion syndrome. *Pediatr. Int.* **56**, 180–187 (2014).

42. Ibayashi, K. *et al.* Estimation of the Number of Patients With Mitochondrial Diseases: A Descriptive Study Using a Nationwide Database in Japan. *J. Epidemiol.* 1–8 (2021) doi:10.2188/jea.je20200577.

43. Bellusci, M. *et al.* The genetic landscape of mitochondrial diseases in spain: A nationwide call. *Genes (Basel).* **12**, (2021).

44. A brief history of Next Generation Sequencing (NGS). https://frontlinegenomics.com/a-brief-history-of-next-generation-sequencing-ngs/.

45. Bannwarth, S. *et al.* Prevalence of rare mitochondrial DNA mutations in mitochondrial disorders. *J. Med. Genet.* **50**, 704–714 (2013).

46. Diogo, L. *et al.* Pediatric Mitochondrial Respiratory Chain Disorders in the Centro Region of Portugal. *Pediatr. Neurol.* **40**, 351–356 (2009).

47. Shoubridge, E. A. Nuclear genetic defects of oxidative phosphorylation. *Hum. Mol. Genet.* **10**, 2277–2284 (2001).

48. Rubio-Gozalbo, M. E. *et al.* Clinical differences in patients with mitochondriocytopathies due to nuclear versus mitochondrial DNA mutations. *Hum. Mutat.* **15**, 522–532 (2000).

49. Sumit, P. M. D. *et al.* A Modern Approach to the Treatment of Mitochondrial Disease. *Curr. Treat. Options Neurol.* **11**, 414–430 (2013).

50. Shantanam, S. & MUELLER. Oxidative Stress in Inherited Mitochondrial Diseases. *Physiol. Behav.* **176**, 139–148 (2018).

51. Tinker, R. J., Lim, A. Z., Stefanetti, R. J. & McFarland, R. Current and Emerging Clinical Treatment in Mitochondrial Disease. *Mol. Diagnosis Ther.* **25**, 181–206 (2021).

52. Martikainen, M. H., Päivärinta, M., Jääskeläinen, S. & Majamaa, K. Successful treatment of POLG-related mitochondrial epilepsy with antiepileptic drugs and low glycaemic index diet. *Epileptic Disord.* **14**, 438–441 (2012).

53. Larsen, F. J. *et al.* Dietary inorganic nitrate improves mitochondrial efficiency in humans. *Cell Metab.* **13**, 149–159 (2011).

54. Klopstock, T., Klopstock, B. & Prokisch, H. Mitochondrial replacement approaches: Challenges for clinical implementation. *Genome Med.* **8**, 8–10 (2016).

55. Ma, H. *et al.* Incompatibility between Nuclear and Mitochondrial Genomes Contributes to an Interspecies Reproductive Barrier. *Cell Metab.* **24**, 283–294 (2016).

56. Mok, B. Y. *et al.* A bacterial cytidine deaminase toxin enables CRISPR-free mitochondrial base editing. *Nature* **583**, 631–637 (2020).

57. Gammage, P. A. *et al.* Genome editing in mitochondria corrects a pathogenic mtDNA mutation in vivo. *Nat. Med.* **24**, 1691–1695 (2018).

58. Bacman, S. R. *et al.* MitoTALEN reduces mutant mtDNA load and restores tRNAAla levels in a mouse model of heteroplasmic mtDNA mutation. *Nat. Med.* **24**, 1696–1700 (2018).

59. Aldossary, A. M. *et al.* Recent advances in mitochondrial diseases: From molecular insights to therapeutic perspectives. *Saudi Pharm. J.* **30**, 1065–1078 (2022).

60. Falkenberg, M. Mitochondrial DNA replication in mammalian cells: Overview of the pathway. *Essays Biochem.* **62**, 287–296 (2018).

61. Chen, Y., Zhang, H., Jenny, H., Ji, W. & Min, W. Mitochondrial redox signaling and tumor progression. *Cancers (Basel).* **8**, 1–15 (2016).

62. Holzerová, E. & Prokisch, H. Mitochondria: Much ado about nothing? How dangerous is reactive oxygen species production? *Int. J. Biochem. Cell Biol.* **63**, 16–20 (2015).

63. Tuppen, H. A. L., Blakely, E. L., Turnbull, D. M. & Taylor, R. W. Mitochondrial DNA mutations and human disease. *Biochim. Biophys. Acta - Bioenerg.* **1797**, 113–128 (2010).

64. Aleksandra Trifunovic *et al.* Premature ageing in mice expressing defective mitochondrial DNA polymerase. *Nature* **429**, 417–423 (2004).

65. Kazak, L., Reyes, A. & Holt, I. J. Minimizing the damage: Repair pathways keep mitochondrial DNA intact. *Nat. Rev. Mol. Cell Biol.* **13**, 659–671 (2012).

66. Puigserver, P. *et al.* A cold-inducible coactivator of nuclear receptors linked to adaptive thermogenesis. *Cell* **92**, 829–839 (1998).

67. Qu, F. C., Xiong, Y., Lupo, E. G., Liu, H. Y. & Cao, W. P38 Mitogen-Activated Protein Kinase Mediates Free Fatty Acid-Induced Gluconeogenesis in Hepatocytes. *J. Biol. Chem.* **281**, 24336–24344 (2006).

68. Fernandez-marcos, P. J. & Auwerx, J. Regulation of PGC-1 a , a nodal regulator of mitochondrial biogenesis 1 – 4. **93**, 884–890 (2011).

69. Miller, K. N. *et al.* Mitochondrial regulator PGC-1a—Modulating the modulator Karl. 37–44 (2020) doi:doi:10.1016/j.coemr.2019.02.002.

70. Youle, R. J. & Van Der Bliek, A. M. Good for Discussion: Mitochondrial Fission, Fusion, and Stress. *Science (80-. ).* **337**, 1062–1065 (2012).

71. Chan, D. C. Fusion and fission: Interlinked processes critical for mitochondrial health. *Annu. Rev. Genet.* **46**, 265–287 (2012).

72. Brunet, S. *et al.* Roles of the Mammalian Mitochondrial Fission and Fusion Mediators Fis1, Drp1, and Opa1 in Apoptosis. *Mol Biol Cell* **15**, 5318–5328 (2004).

73. Waterham, H. R. *et al.* A Lethal Defect of Mitochondrial and Peroxisomal Fission. *N. Engl. J. Med.* **356**, 1736–1741 (2007).

74. Amati-Bonneau, P. *et al.* OPA1 mutations induce mitochondrial DNA instability and optic atrophy 'plus' phenotypes. *Brain* **131**, 338–351 (2008).

75. Tondera, D. *et al.* SlP-2 is required for stress-induced mitochondrial hyperfusion. *EMBO J.* **28**, 1589–1600 (2009).

76. Gomes, L. C., Benedetto, G. Di & Scorrano, L. During autophagy mitochondria elongate, are spared from degradation and sustain cell viability. *Nat. Cell Biol.* **13**, 589–598 (2011).

77. Onishi, M. & Okamoto, K. Mitochondrial clearance: mechanisms and roles in cellular fitness. *FEBS Lett.* **595**, 1239–1263 (2021).

78. Palikaras, K., Lionaki, E. & Tavernarakis, N. Mechanisms of mitophagy in cellular homeostasis, physiology and pathology. *Nat. Cell Biol.* **20**, 1013–1022 (2018).

79. Pryde, K. R., Smith, H. L., Chau, K. Y. & Schapira, A. H. V. PINK1 disables the anti-fission machinery to segregate damaged mitochondria for mitophagy. *J. Cell Biol.* **213**, 163–171 (2016).

80. Whitworth, A. J. & Pallanck, L. J. PINK1/Parkin mitophagy and neurodegeneration—what do we really know in vivo? *Curr. Opin. Genet. Dev.* **44**, 47–53 (2017).

81. Kang, R. *et al.* A novel PINK1- and PARK2-dependent protective neuroimmune pathway in lethal sepsis. *Autophagy* **12**, 2374–2385 (2016).

82. Liu, L. *et al.* Mitochondrial outer-membrane protein FUNDC1 mediates hypoxia-induced mitophagy in mammalian cells. **14**, (2012).

83. Julien, O. & Wells, J. A. Caspases and their substrates. *Cell Death Differ.* **24**, 1380–1389 (2017).

84. Boatright, K. M. *et al.* A unified model for apical caspase activation. *Mol. Cell* **11**, 529–541 (2003).

85. Ow, Y. L. P., Green, D. R., Hao, Z. & Mak, T. W. Cytochrome c: Functions beyond respiration. *Nat. Rev. Mol. Cell Biol.* **9**, 532–542 (2008).

86. Bock, F. J. & Tait, S. W. G. Mitochondria as multifaceted regulators of cell death. *Nat. Rev. Mol. Cell Biol.* **21**, 85–100 (2020).

87. Shi, Y. Apoptosome Assembly. **442**, 141–156 (2008).

88. Dorstyn, L., Akey, C. W. & Kumar, S. New insights into apoptosome structure and function. *Cell Death Differ.* **25**, 1194–1208 (2018).

89. Patil, C. & Walter, P. Intracellular signaling from the endoplasmic reticulum to the nucleus: The unfolded protein response in yeast and mammals. *Curr. Opin. Cell Biol.* **13**, 349–355 (2001).

90. Zhao, Q. *et al.* A mitochondrial speci®c stress response in mammalian cells. **21**, 4411–4419 (2002).

91. Coates, D. R., Chin, J. M. & Chung, S. T. L. Mitochondrial Import Efficiency of ATFS-1 Regulates Mitochondrial UPR Activation. *Bone* **23**, 1–7 (2011).

92. Gustavson, D. E. & Miyake, A. Mitochondrial and nuclear accumulation of the transcription factor ATFS-1 promotes OXPHOS recovery during the UPRmt. *Cogn. Emot. J.* **30**, 1289–1303 (2016).

93. Fiorese, C. J. *et al.* The Transcription Factor ATF5 Mediates a Mammalian Mitochondrial UPR. *Curr. Biol.* **26**, 2037–2043 (2016).

94. Zhou, D. *et al.* Phosphorylation of eIF2 directs ATF5 translational control in response to diverse stress conditions. *J. Biol. Chem.* **283**, 7064–7073 (2008).

95. Baker, B. M., Nargund, A. M., Sun, T. & Haynes, C. M. Protective coupling of mitochondrial function and protein synthesis via the eIF2α kinase GCN-2. *PLoS Genet.* **8**, (2012).

96. Liu, S., Liu, S. & Jiang, H. Multifaceted roles of mitochondrial stress responses under ETC dysfunction – repair , destruction and pathogenesis. **289**, 6994–7013 (2022).

97. Suomalainen, A. & Battersby, B. J. Mitochondrial diseases: The contribution of organelle stress responses to pathology. *Nat. Rev. Mol. Cell Biol.* **19**, 77–92 (2018).

98. Mick, E. *et al.* Distinct mitochondrial defects trigger the integrated stress response depending on the metabolic state of the cell. *Elife* **9**, (2020).

99. Forsström, S. *et al.* Fibroblast Growth Factor 21 Drives Dynamics of Local and Systemic Stress Responses in Mitochondrial Myopathy with mtDNA Deletions. *Cell Metab.* **30**, 1040-1054.e7 (2019).

100. Fessler, E. *et al.* A pathway coordinated by DELE1 relays mitochondrial stress to the cytosol. *Nature* **579**, 433–437 (2020).

101. Guo, X. *et al.* Mitochondrial stress is relayed to the cytosol by an OMA1–DELE1–HRI pathway. *Nature* **579**, 427–432 (2020).

102. Ahola, S. *et al.* OMA1-mediated integrated stress response protects against ferroptosis in mitochondrial cardiomyopathy. *Cell Metab.* 1–17 (2022) doi:10.1016/j.cmet.2022.08.017.

103. Zhang, G. *et al.* Integrated Stress Response Couples Mitochondrial Protein Translation With Oxidative Stress Control. *Circulation* **144**, 1500–1515 (2021).

104. Croon, M. *et al.* FGF21 modulates mitochondrial stress response in cardiomyocytes only under mild mitochondrial dysfunction. *Sci. Adv.* **8**, 1–16 (2022).

105. Harding, H. P. *et al.* An integrated stress response regulates amino acid metabolism and resistance to oxidative stress. *Mol. Cell* **11**, 619–633 (2003).

106. Kruse, S. E. *et al.* Mice with Mitochondrial Complex I Deficiency Develop a Fatal

Encephalomyopathy. *Cell Metab.* **7**, 312–320 (2008).

107. Quintana, A., Kruse, S. E., Kapur, R. P., Sanz, E. & Palmiter, R. D. Complex I deficiency due to loss of Ndufs4 in the brain results in progressive encephalopathy resembling Leigh syndrome. *Proc. Natl. Acad. Sci. U. S. A.* **107**, 10996–11001 (2010).

108. Ke, B. X. *et al.* Tissue-specific splicing of an Ndufs6 gene-trap insertion generates a mitochondrial complex I deficiency-specific cardiomyopathy. *Proc. Natl. Acad. Sci. U. S. A.* **109**, 6165–6170 (2012).

109. Van Rossum, G. & Drake, F. L. Python 3 Reference Manual; CreateSpace. *Scotts Val. CA* 242 (2009).

110. Sultana, S., Sarker, S. A. & Brüssow, H. SCANPY: large-scale single-cell gene expression data analysis. *Environ. Microbiol.* **19**, 2926–2934 (2017).

111. Wolf, F. A. *et al.* PAGA: graph abstraction reconciles clustering with trajectory inference through a topology preserving map of single cells. *Genome Biol.* **20**, 1–9 (2019).

112. Johnson, W. E., Li, C. & Rabinovic, A. Adjusting batch effects in microarray expression data using empirical Bayes methods. *Biostatistics* **8**, 118–127 (2007).

113. Kuleshov, M. V. *et al.* Enrichr: a comprehensive gene set enrichment analysis web server 2016 update. *Nucleic Acids Res.* **44**, W90–W97 (2016).

114. Xie, Z. *et al.* Gene Set Knowledge Discovery with Enrichr. *Curr. Protoc.* **1**, (2021).

115. Ge, S. X., Son, E. W. & Yao, R. iDEP: an integrated web application for differential expression and pathway analysis of RNA-Seq data. *BMC Bioinforma. 2018 191* **19**, 1–24 (2018).

116. Hammelman, J., Patel, T., Closser, M., Wichterle, H. & Gifford, D. Ranking reprogramming factors for cell differentiation. *Nat. Methods 2022 197* **19**, 812–822 (2022).

117. Hunter, J. D. : a 2D G. *Comput. Sci. Eng.* **9**, 90–95 (2007).

118. Mcinnes, L., Healy, J. & Melville, J. UMAP: Uniform Manifold Approximation and Projection for Dimension Reduction. (2020).

119. Traag, V. A., Waltman, L. & van Eck, N. J. From Louvain to Leiden: guaranteeing well-connected communities. *Sci. Rep.* **9**, 1–12 (2019).

120. Jacomy, M., Venturini, T., Heymann, S. & Bastian, M. ForceAtlas2, a Continuous Graph Layout Algorithm for Handy Network Visualization Designed for the Gephi Software. *PLoS One* **9**, e98679 (2014).

121. Kim, D., Paggi, J. M., Park, C., Bennett, C. & Salzberg, S. L. Graph-based genome alignment and genotyping with HISAT2 and HISAT-genotype. *Nat. Biotechnol.* **37**, 907–915 (2019).

122. Martelotto, L. 'Frankenstein' protocol for nuclei isolation from fresh and frozen tissue for snRNAseq. *protocols.io* (2020).

123. Honda, M. *et al.* High-depth spatial transcriptome analysis by photo-isolation chemistry. *Nat. Commun.* **12**, 1–11 (2021).

124. Honda, M. *et al.* Photo-isolation chemistry for high-resolution and deep spatial transcriptome with mouse tissue sections. *STAR Protoc.* **3**, 101346 (2022).

125. Fujihara, Y. *et al.* Identification of multiple male reproductive tractspecific proteins that regulate sperm migration through the oviduct in mice. *Proc. Natl. Acad. Sci. U. S. A.* **116**, 18498–18506 (2019).

126. Logan, P. G. B. and G. D. *et al.* Differential Contribution of Monocytes to Heart Macrophages in Steady-State and after Myocardial Infarction. *Bone* **23**, 1–7 (2014).

127. Mescher, A. L. Macrophages and fibroblasts during inflammation and tissue repair in models of organ regeneration. *Regeneration* **4**, 39–53 (2017).

128. Hai T, Wolfgang CD, Marsee DK, Allen AE, S. U. ATF3 and stress responses. *Gene Expr.* **7**, 321–335 (1999).

129. Lin, H. *et al.* Activating transcription factor 3 protects against pressure-overload heart failure via the autophagy molecule Beclin-1 pathway. *Mol. Pharmacol.* **85**, 682–691 (2014).

130. Brooks, A. C. *et al.* Induction of activating transcription factor 3 limits survival following infarct-induced heart failure in mice. *Am. J. Physiol. - Hear. Circ. Physiol.* **309**, H1326–H1335 (2015).

131. Li, Y. *et al.* Cardiac fibroblast-specific activating transcription factor 3 protects against heart failure by suppressing MAP2K3-p38 signaling. *Circulation* **135**, 2041–2057 (2017).

132. Koren, L., Elhanani, O., Kehat, I., Hai, T. & Aronheim, A. Adult Cardiac Expression of the Activating Transcription Factor 3, ATF3, Promotes Ventricular Hypertrophy. *PLoS One* **8**, 1–10 (2013).

133. Jia, Y. *et al.* Cardiomyocyte-Specific Ablation of Med1 Subunit of the Mediator Complex Causes Lethal Dilated Cardiomyopathy in Mice. *PLoS One* **11**, 1–24 (2016).

134. Zhou, H. *et al.* ATF3 regulates multiple targets and may play a dual role in cardiac hypertrophy and injury. *Int. J. Cardiol.* **174**, 838–839 (2014).

135. Lin, H. & Cheng, C. F. Activating transcription factor 3, an early cellular adaptive responder in ischemia/reperfusion-induced injury. *Tzu Chi Med. J.* **30**, 61–65 (2018).

136. Liu, Y., Hu, Y., Xiong, J. & Zeng, X. Overexpression of Activating Transcription Factor 3 Alleviates Cardiac Microvascular Ischemia/Reperfusion Injury in Rats. *Front. Pharmacol.* **12**, 1–17 (2021).

137. Yang, C. J., Yang, J., Fan, Z. X. & Yang, J. Activating transcription factor 3 - An endogenous inhibitor of myocardial ischemia-reperfusion injury (Review). *Mol. Med. Rep.* **13**, 9–12 (2016).

138. Thompson, M. R., Xu, D. & Williams, B. R. G. ATF3 transcription factor and its emerging roles in immunity and cancer. *J. Mol. Med.* **87**, 1053–1060 (2009).

139. Li, H. F., Cheng, C. F., Liao, W. J., Lin, H. & Yang, R. B. ATF3-mediated epigenetic regulation protects against acute kidney injury. *J. Am. Soc. Nephrol.* **21**, 1003–1013 (2010).

140. Yin, T. *et al.* Tissue-specific pattern of stress kinase activation in ischemic/reperfused

heart and kidney. *J. Biol. Chem.* **272**, 19943–19950 (1997).

141. Rao, J. *et al.* ATF3-mediated NRF2/HO-1 signaling regulates TLR4 innate immune responses in mouse liver ischemia/reperfusion injury. *Am. J. Transplant.* **15**, 76–87 (2015).

142. Zhu, Q. *et al.* Loss of ATF3 exacerbates liver damage through the activation of mTOR/p70S6K/ HIF-1α signaling pathway in liver inflammatory injury. *Cell Death Dis.* **9**, 1–13 (2018).

143. Ghigo, A., Frati, G. & Sciarretta, S. A novel protective role for activating transcription factor 3 in the cardiac response to metabolic stress. *Cardiovasc. Res.* **113**, 113–114 (2017).

144. Zhou, H. *et al.* Activating transcription factor 3 in cardiovascular diseases: a potential therapeutic target. *Basic Res. Cardiol.* **113**, 1–13 (2018).

145. Morris, E. M. *et al.* PGC-1 ⎵ overexpression results in increased hepatic fatty acid oxidation with reduced triacylglycerol accumulation and secretion. 979–992 (2022) doi:10.1152/ajpgi.00169.2012.

146. Gore, J. L., Nunan, E., Wright, C. & Butcher, J. T. PGC1α Overexpression Protects against Cardio-Metabolic Disease and Skeletal Muscle Dysfunction in a Type 2 Diabetic Mouse Model. *FASEB J.* **36**, (2022).

147. Wong, K. E. *et al.* Muscle-Speci fi c Overexpression of PGC-1 a Does Not Augment Metabolic Improvements in Response to Exercise and Caloric Restriction. **64**, 1532–1543 (2015).

148. Liang, H. *et al.* Whole body overexpression of PGC-1α has opposite effects on hepatic and muscle insulin sensitivity. *Am. J. Physiol. - Endocrinol. Metab.* **296**, (2009).

149. Yatsuga, S. & Suomalainen, A. Effect of bezafibrate treatment on late-onset mitochondrial myopathy in mice. *Hum. Mol. Genet.* **21**, 526–535 (2012).

150. Viscomi, C. *et al.* In vivo correction of COX deficiency by activation of the AMPK/PGC-1α axis. *Cell Metab.* **14**, 80–90 (2011).

151. Receptor, C. P. P. *et al.* Cardiac-Specific Induction of the Transcriptional Reversible Cardiomyopathy in a Developmental. (2004) doi:10.1161/01.RES.0000117088.36577.EB.

152. Lehman, J. J. *et al.* Peroxisome proliferator – activated receptor γ coactivator-1 promotes cardiac mitochondrial biogenesis Find the latest version : Peroxisome proliferator – activated receptor γ coactivator-1 promotes cardiac mitochondrial biogenesis. **106**, 847–856 (2000).

153. Huang, P. *et al.* Fine-Tuning of PGC1 α Expression Regulates Cardiac Function and Longevity. 707–719 (2019) doi:10.1161/CIRCRESAHA.119.315529.

154. Lehtonen, J. M., Viscomi, C., Baris, O. R. & Isoniemi, H. FGF21 is a biomarker for mitochondrial translation and mtDNA maintenance disorders. (2016) doi:10.1212/WNL.0000000000003374.

# Academic achievements

## Academic papers

1. Qaqorh T, Nishida Y, Takahashi Y, Yazawa I, Matsuoka K, Thorburn D, Ohtani K, Honda M, Oki S, Yamazaki S, Fujihara Y, Takashima S, Shintani Y. Single cell transcriptomics reveals a fate transitioning factor of cardiomyocytes in mitochondrial cardiomyopathy 投稿準備中

2. Nishida Y, Yanagisawa S, Morita R, Shigematsu H, Shinzawa-Itoh K, Yuki H, Ogasawara S, Shimuta K, Iwamoto T, Nakabayashi C, Matsumura W, Kato H, Gopalasingam C, Nagao T, Qaqorh T, Takahashi Y, Yamazaki S, Kamiya K, Harada R, Mizuno N, Takahashi H, Akeda Y, Ohnishi M, Ishii Y, Kumasaka T, Murata T, Kazumasa Muramoto K, Takehiko Tosha T, Yoshitsugu Shiro Y, Teruki Honma T, Shigeta Y, Kubo M, Takashima S, Shintani Y (2022) Identifying antibiotics based on structural differences in the conserved allostery from mitochondrial heme-copper oxidases. *Nat. Commun.* 13(1) 7591-7591

3. Yashirogi S, Nagao T, Nishida Y, Takahashi Y, Qaqorh T, Yazawa I, Katayama T, Kioka H, Matsui T, Saito S, Masumura Y, Tsukamoto O, Kato H, Ueda H, Yamaguchi O, Yashiro K, Yamazaki S, Takashima S, Shintani Y (2021) AMPK regulates cell shape of cardiomyocytes by modulating turnover of microtubules through CLIP-170. *EMBO rep* 22: e50949

## Conference presentations

1. **Mitochondrial cardiomyopathy disease model at a single-cell resolution**
   The 20th Conference of Japanese Society of Mitochondrial Research and Medicine
   Gakushuin University, Tokyo, Japan
   2021.12.9-10
   Oral presentation

2. **Mitochondrial cardiomyopathy disease model at a single-cell resolution**
   21st European Bioenergetics Conference
   Aix-Marseille University, Aix-en-Provence, France
   2022.8.20-25
   Poster presentation

3. **Mitochondrial cardiomyopathy disease model at a single-cell resolution**
   Cell Symposia – Multifaceted Mitochondria
   Seville, Spain
   2022.11.6-8
   Poster presentation